Differential Movement Across Byrd Glacier,

Transantarctic Mountains, Antarctica as Indicated by

(U-Th)/He Thermochronology and Geomorphology

by

Daniel Joseph Foley

A Thesis Presented in Partial Fulfillment
of the Requirements for the Degree
Master of Science

Approved April 2011 by the
Graduate Supervisory Committee:

Edmund Stump, Chair
Kelin Whipple
Kip Hodges

ARIZONA STATE UNIVERSITY

May 2011

ABSTRACT

The Byrd Glacier region of Antarctica is important for understanding the tectonic development and landscape evolution of the Transantarctic Mountains (TAM). This outlet glacier crossing the TAM marks a major discontinuity in the Neoproterozoic-early Paleozoic Ross orogen. The region has not been geologically mapped in detail, but previous studies have inferred a fault to exist beneath and parallel to the direction of flow of Byrd Glacier. Thermochronologic analysis has never been undertaken across Byrd Glacier, and little is known of the exhumation history of the region. The objectives of this study are to assess possible differential movement across the inferred Byrd Glacier fault, to measure the timing of exhumation, and to gain a better overall understanding of the structural architecture of the TAM.

Apatites and zircons separated from rock samples collected from various locations north and south of Byrd Glacier were dated using single-crystal (U-Th)/He analysis. Similar cooling histories were revealed with comparable exhumation rates of 0.03 ± 0.003 and 0.04 ± 0.03 mm/yr north and south of Byrd Glacier from apatite data and somewhat similar rates of 0.06 ± 0.008 and 0.04 ± 0.01 mm/yr north and south of Byrd Glacier from zircon data. Age vs. elevation regressions indicate a vertical offset of 1379 ± 159 m and 4000 ± 3466 m from apatite and zircon data.

To assess differential movement, the Kukri Peneplain (a regional unconformity) was utilized as a datum. On-site photographs, Landsat imagery, and Aster Global DEM data were combined to map Kukri Peneplain elevation

points north and south of Byrd Glacier. The difference in elevation of the peneplain as projected across Byrd Glacier shows an offset of 1122 ± 4.7 m.

This study suggests a model of relatively uniform exhumation followed by fault displacement that uplifted the south side of Byrd Glacier relative to the north side. Combining apatite and zircon (U-Th)/He analysis along with remote geomorphologic analysis has provided an understanding of the differential movement and exhumation history of crustal blocks in the Byrd Glacier region. The results complement thermochronologic and geomorphologic studies elsewhere within the TAM providing more information and a new approach.

To my Mom and Dad who always believed in me and who were always there for me.

ACKNOWLEDGEMENTS

I would like to thank Ed Stump for serving as my advisor and for guidance with research, interpretations and writing, his excellent insight and support have proved invaluable in this Masters Thesis. Special thanks to Ed Stump for sticking with me on this project and taking me to Antarctica. I would like to thank Kelin Whipple and Kip Hodges for their expertise in serving on my committee. I would like to thank Brian Monteleone for help with rock processing and mineral extraction procedures in preparation for thermochronology analysis. I would like to thank Matthijs van Soest for help with (U-Th)/He thermochronology methods, procedures, analysis, and interpretations. I would like to thank Mike Zoldak for help with Arc GIS and DEM processing in geomorphological analysis. I would like to thank Byron Adams and Alka Tripathy for help with Matlab codes and statistical analysis.

TABLE OF CONTENTS

Page

LIST OF TABLES

LIST OF FIGURES

INTRODUCTION

The Byrd Glacier region of the Transantarctic Mountains (TAM) is important for understanding the tectonic development and landscape evolution of Antarctica (Figures 1 and 2). This ~ 24 km wide major outlet glacier crossing the TAM at approximately 80.00^{o} S latitude and 159.00^{o} E longitude marks a major discontinuity in the Neoproterozoic-early Paleozoic Ross orogen with upper amphibolite grade metamorphics and granites to the north and lower grade greenschist metamporphics and limestones to the south of Byrd Glacier (Figures 3 and 4). The region has not been mapped in detail geologically, but previous studies have postulated that a fault exists beneath Byrd Glacier (Grindley and Laird, 1969). Previous apatite fission track studies in other parts of the TAM have revealed evidence of a major pulse of exhumation at ~ 50 Ma. However, thermochronologic analysis has never been done across Byrd Glacier and little is known of the differential exhumation history across the postulated fault beneath Byrd Glacier. The objectives of this study are 1) to evaluate the evidence for possible displacement across the inferred Byrd Glacier fault; 2) to estimate the amount of throw on the fault if such evidence is found; and 3) to better understand the exhumation history of this relatively unknown part of the TAM.

This project combines thermochronologic and geomorphologic analytical methods to study the Byrd Glacier region of the TAM. The thermochronologic work employs apatite and zircon (U-Th)/He thermochronometry. Geomorphic reconstructions were based on the Kukri Peneplain: an unconformity visible across Byrd Glacier with Proterozoic to early Paleozoic basement rocks of the Ross Orogen overlain by Devonian to Triassic sedimentary rocks of the Beacon Supergroup. As this erosional surface was likely at a relatively uniform elevation at the time of its formation, mapping the elevation north and south of Byrd Glacier was utilized to quantify displacement.

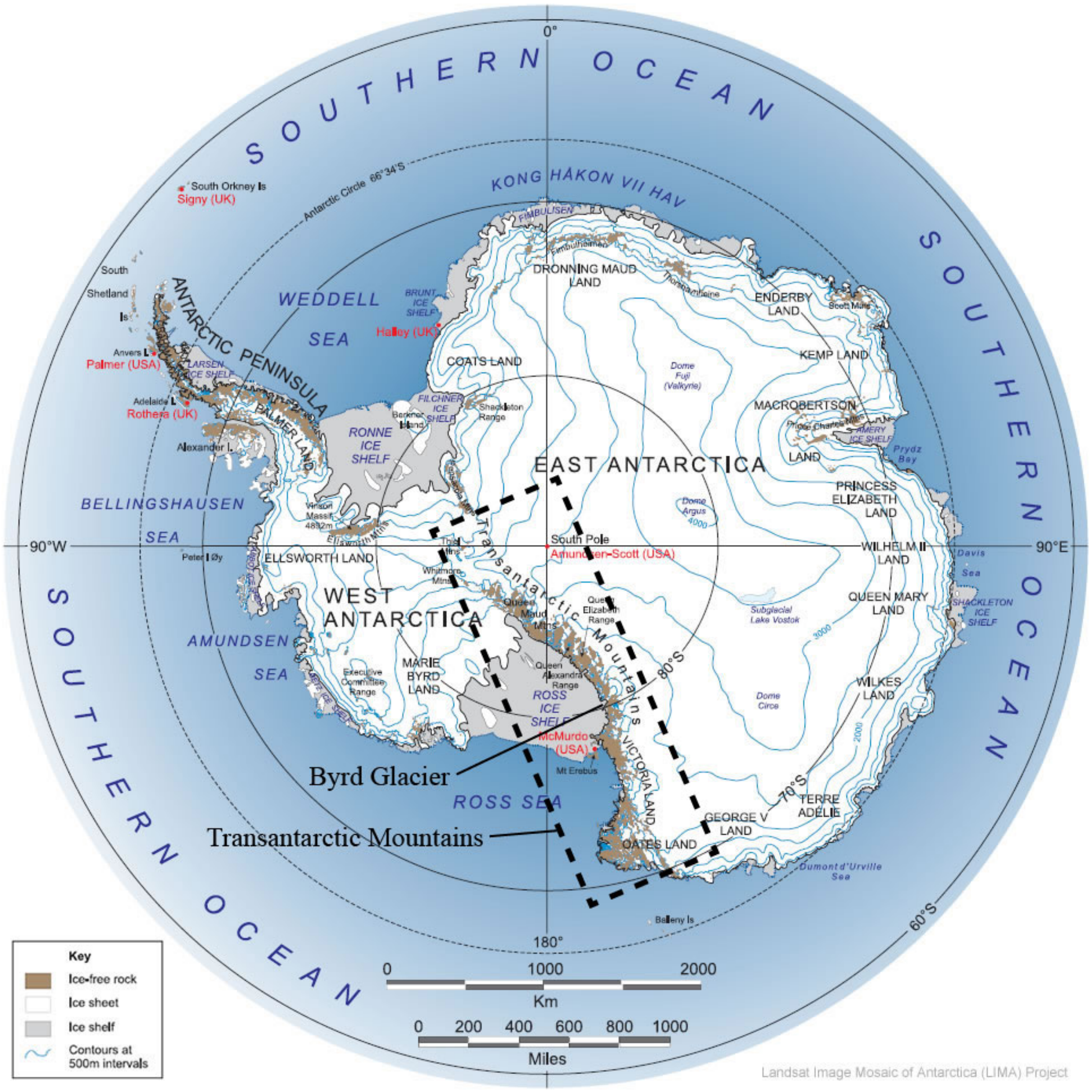

Figure 1. Antarctica overview map with Transantarctic Mountains and Byrd Glacier labeled. Modified image courtesy of British Antarctic Survey.

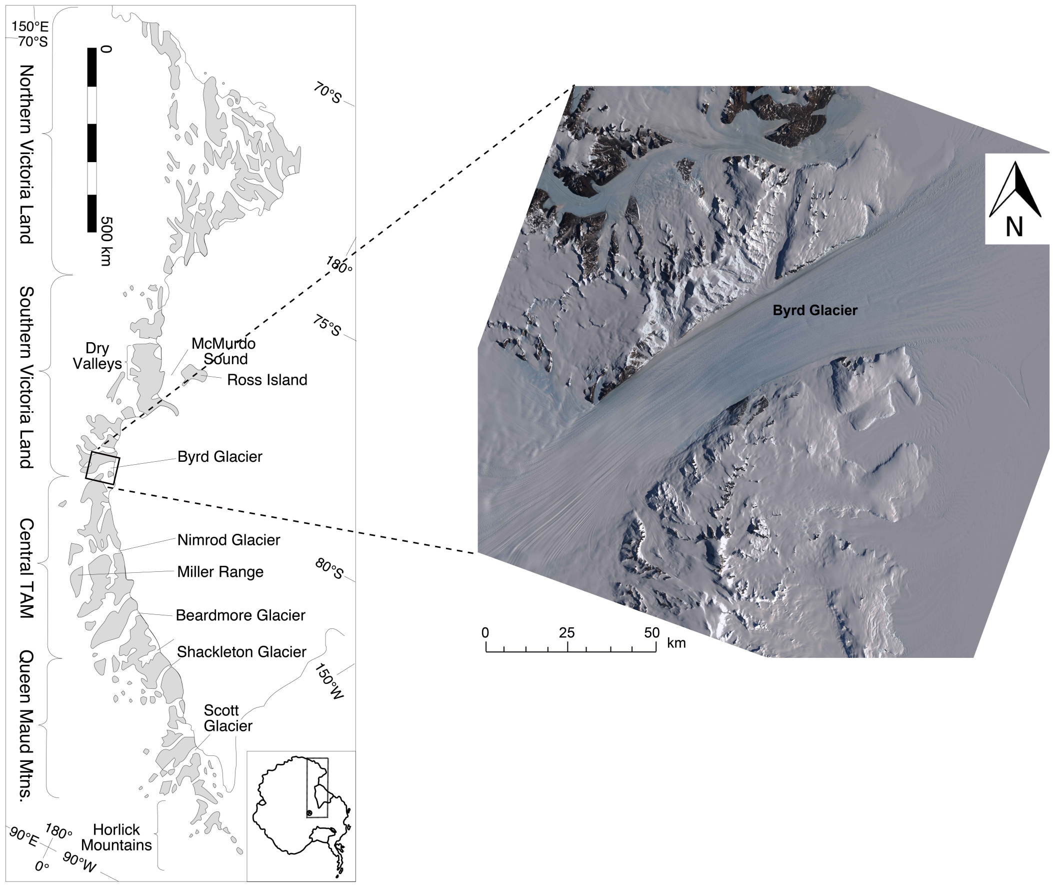

Figure 2. Location maps of the Transantarctic Mountains with a detail of Byrd Glacier.

Figure 3. Byrd Glacier, Transantarctic Mountains, Antarctica. View is from the south toward the Britannia Range. Shackleton Limestone crops out in the foreground to the east of Mt. Tuatara. Photo by Ed Stump.

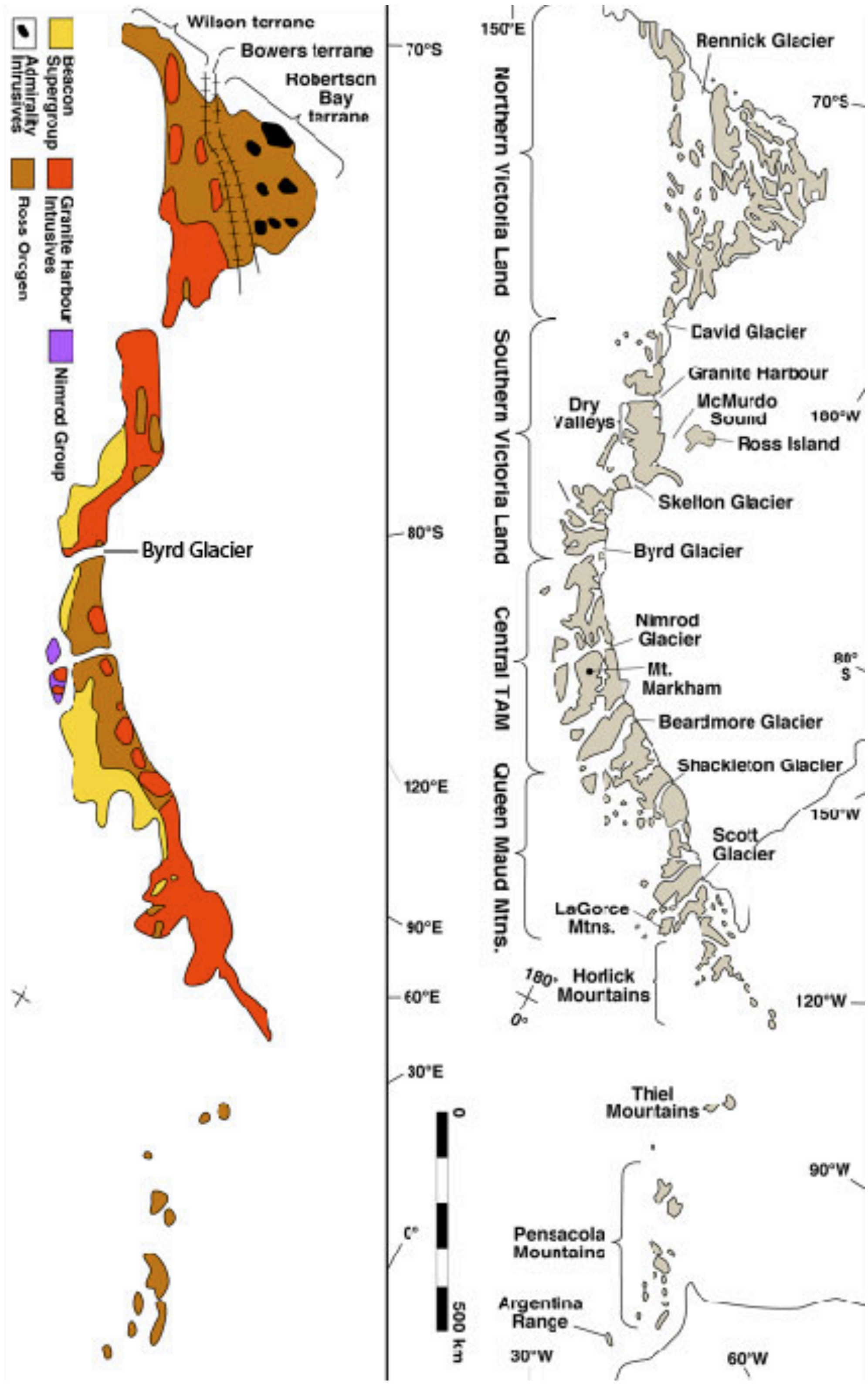

Figure 4. Byrd Glacier Discontinuity Map.

BACKGROUND

Transantarctic Mountains Geology

The TAM are an intracontinental range 3500 kilometers in length that span throughout the entirety of Antarctica. They reach elevations greater than 4000 meters providing the most extensive rock outcrop anywhere on the continent (Figure 5). Forming the morphological and geological boundary between East and West Antarctica, they are the uplifted shoulder of the Cretaceous-Cenozoic West Antarctic Rift system.

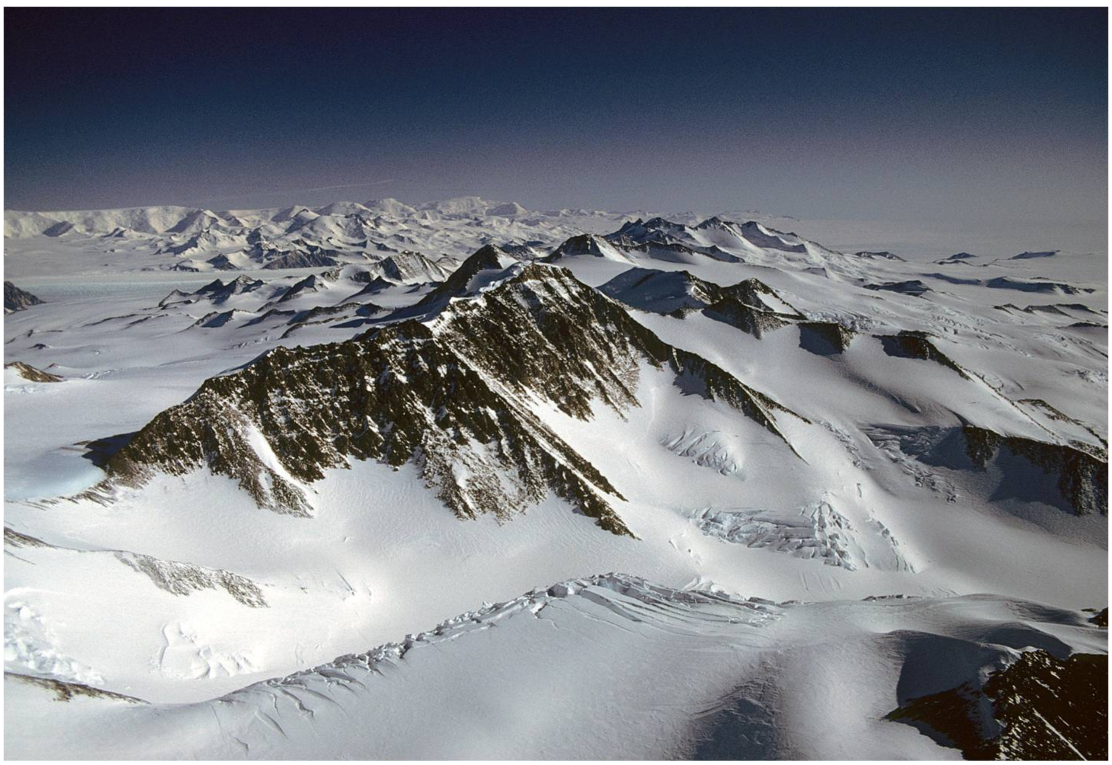

Figure 5. Queen Maud Mountains, Transantarctic Mountains, Antarctica. Seen from Mt. Griffith across Amundsen Glacier to Mt. Fridtjof Nansen at center skyline. Polar plateau marks left skyline and Ross Ice Shelf marks right skyline. Photo by Ed Stump.

Precambrian and Cambrian metasedimentary rocks and metavolcanic rocks together with Cambro-Ordovician plutonic rocks of the Granite Harbour Intrusives and the Devonian Admiralty Intrusives form the basement rocks of the TAM. This basement was exhumed as much as 15 – 20 kilometers prior to the Devonian and eroded to form the Kukri Peneplain during the Ordovician to Silurian (Grindley and Laird, 1969). Subsequently the unconformity was overlain by the shallow marine, glacial, and alluvial plain sediments of the Devonian-Triassic Beacon Supergroup. In the Jurassic, tholeiitic magmatism produced sills of the Ferrar Dolerite and lava flows of the Kirkpatrick Basalt throughout the TAM (Fitzgerald, 1992). $^{40}Ar/^{39}Ar$ analysis of the Ferrar Dolerite indicates that it was intruded at 176.6 ± 1.8 Ma during an episode that lasted less than 1 million years (Fleming et al., 1997).

The Jurassic magmatism was pervasive, spanning over 3000 kilometers of the TAM with sills as thick as 1000 meters. Apatite fission track (AFT) studies have shown that the accompanying thermal pulse was sufficient to totally anneal apatites everywhere in the TAM except at three localities adjacent to the East Antarctic Ice Sheet where apatite escaped the thermal overprinting. These include the Lichen Hills and Outback Nunatuks in northern Victoria Land (Fitzgerald and Gleadow, 1988), and the Miller Range in the central TAM (Fitzgerald, 1994).

Apatite fission track thermochronology. In order to better understand the landscape tectonic and morphologic evolution, AFT is important to quantify the timing of development of topography. The exhumation history of the present TAM is an important geologic question that has been addressed by AFT analysis, and more recently apatite (U-Th)/He analysis.

AFT ages have been observed to increase with increasing elevation. This is explained by the concept of a column of rock passing through the closure temperature of apatite during exhumation. For this study, exhumation is defined as the upward movement of rock with respect to Earth's surface, and surface uplift is defined as upward movement of the surface with respect to a fixed datum, e.g. mean sea level (England and Molnar, 1990).

AFT dating is based on the analysis of tracks produced by fission fragments of ^{238}U that damage the crystal structure of the mineral apatite. Fission tracks are preserved in apatite when the ambient temperature of the rock falls below the annealing temperature of approximately 110° C. Because ^{238}U undergoes spontaneous fission at a known rate, the timing of cooling below the closure temperature can be determined. Through the sampling of vertical profiles, fission-track thermochronology provides insight into the timing, amount, and rate of denudation of mountain ranges. Vertical sampling profiles involve the collection of rock samples over the largest possible vertical interval. As discussed below, AFT analysis has previously been applied to four major regions of the TAM, including northern Victoria Land, southern Victoria Land, the central TAM, and the Queen Maud Mountains (Figure 2).

Southern Victoria Land. The occurrence and pattern of differential exhumation across the TAM can be estimated from the vertical offsets of different AFT age profiles sampled across southern Victoria Land (SVL). These show the structure of the mountain range to be that of a large tilt block, dipping gently to the west under the polar ice cap and bounded by a major fault zone on its eastern side (Gleadow and Fitzgerald 1987).

An apatite age profile from Mount England records a "break in slope" in an age vs. elevation diagram indicating rapid cooling from inferred exhumation began at ~ 55 Ma (Fitzgerald, 1992). Horizontal sampling traverses, in addition to field mapping provide insight into the structure of the TAM front as a zone of north-south striking, steeply-dipping, normal faults with displacements of 40 – 1000 meters dominantly down to the east. Results from Fitzgerald (1992) have shown that the amount of exhumation decreases to the west at the same rate as the decrease in dip of the Kukri Peneplain and that the amount of erosion decreases more as indicated by the increasing height of the mountains to the west. Offset dolerite sills at Mt. Doorly show the mountain front to be displaced by 1000 meters or more down to the coast from an axis of maximum uplift just inland from Mt. Doorly (Gleadow and Fitzgerald, 1987).

Northern Victoria Land. By comparison, AFT results from northern Victoria Land (NVL) indicate a two-stage exhumation history, although a variety of thermal histories exist for different parts of NVL (Fitzgerald and Gleadow, 1988). A pronounced "break in slope" in the AFT apatite age-elevation profile for results from most of NVL occurs at ~ 50 Ma, corresponding to the start of accelerated exhumation in NVL (Fitzgerald and Gleadow, 1988). At unusual localities on the western margin of NVL, apatites have not been completely overprinted by the Jurassic thermal event associated with emplacement of the Ferrar Dolerite. These include ages of ~ 315 Ma from the Lichen Hills, and ~ 196-251 Ma from the Outback Nunataks (Fitzgerald and Gleadow, 1988).

Central Transantarctic Mountains. Fitzgerald (1994) has shown fault blocks are discernible in present-day topography and subglacial morphology of the central TAM. Exhumation patterns are similar to those determined for other parts of the TAM for exhumation initiated in the early Cenozoic, but they are complicated by an Early Cretaceous exhumation pulse which appears to be present along the inland edge of inland blocks. AFT thermochronology on samples collected from the central TAM record a complex multi-phase thermotectonic history for this region over the past 350 million years. Apatite ages in the Miller Range escaped the Jurassic thermal event and vary from ~ 250 – 350 Ma. They record an exhumed apatite partial annealing zone formed following cooling of Cambro-Ordovician granitoids. A period of Early Cretaceous exhumation (<2 kilometer), beginning at ~ 115 Ma, is recorded at Moody Nunatak on the inland side of the TAM (Fitzgerald, 1994). Near the coast, samples between the Nimrod and Beardmore Glaciers and along the Beardmore Glacier record rapid cooling indicative of exhumation initiated in the early Cenozoic at ~ 50 Ma (Fitzgerald, 1992). Consistent with SVL, the Cenozoic exhumation inferred uplift is greatest near the coast and decreases inland.

Queen Maud Mountains. The AFT data from the Scott Glacier area of the Queen Maud Mountains suggest at least three periods of exhumation: Early Cretaceous (initiated at ~ 125 Ma), Late Cretaceous (initiated at ~ 95 Ma), and early Cenozoic (initiated at 50 – 45 Ma) (Fitzgerald and Stump, 1997). Patterns in age profiles indicate that the episodes of exhumation in the Early Cretaceous, Late Cretaceous, and Cenozoic were separated by periods of relative tectonic stability. Also, consistent with other regions studied by AFT thermochronology, exhumation was a maximum along the coast, and decreased inland. Patterns of rock uplift and denudation are complicated by Cenozoic faulting, mostly by structures oriented ~ 45^{o} to the TAM front (Fitzgerald and Stump, 1997).

Within the broad regional context, the Cretaceous was a time of continental breakup in this sector of Gondwana (Stump and Fitzgerald, 1992). The three periods of exhumation recorded in age profiles in the Scott Glacier region can be related to regional tectonic events: Early Cretaceous southward translation of the Ellsworth-Whitmore Mountains block of West Antarctica relative to East Antarctica; Late Cretaceous extension in the Ross embayment between East and West Antarctica, and early Cenozoic rejuvenated faulting, magmatism, and deformation within the Victoria Land Basin and its presumed southward extension under the Ross Ice Shelf (Fitzgerald and Stump, 1997).

The early Cenozoic episode affected the TAM throughout the sector of the Ross Embayment, whereas the Cretaceous episodes were not so extensive (Stump and Fitzgerald, 1992). The major phase of rock uplift and denudation responsible for the present day TAM was initiated in the early Cenozoic. The amount of denudation since the early Cenozoic decreases across the TAM from maximum of ~ 6 kilometers near the coast (Fitzgerald, 1992).

Apatite and Zircon (U-Th)/He thermochronology. (U–Th)/He dating, based on the decay of uranium and thorium via the production of α-particles (^{4}He nuclei), has been shown to be an important thermochronometer in interpreting cooling histories (Farley, 2002; Zeitler et al., 1987). This method has been applied by Fitzgerald et al. (2006) to two vertical profiles in SVL at Cathedral Rocks and Peak 1880 on opposite sides of the Ferrar Glacier, where comparison was made with well-constrained AFT analyses (Fitzgerald et al., 2006). Results show that cooling histories of AFT ages vary systematically with elevation at Cathedral Rocks with ages from ~ 50 - 92 Ma and at Peak 1880 with ages from ~ 43 - 66 Ma. Apatite (U–Th)/He single-grain ages are not as systematic with considerable intra-sample age variation. This variation has been attributed to complicating factors associated with the (U–Th)/He method, such as U- and Th-rich (micro) inclusions, fluid inclusions, variation in crystal size, α-particle ejection, α-particle ejection correction, zonation, implantation of He into a crystal, impediment of He diffusion out of a crystal by crystal defects, and ^{147}Sm-derived α-particles (Fitzgerald et al., 2006). At Cathedral Rocks ages range between ~ 36 - 274 Ma (or ~ 36 – 57 Ma when three significantly older grains are excluded due to likely undetected U-Th inclusions). At Peak 1880, ages vary from ~ 34 - 57 Ma. The combined data of the two profiles indicate a similar episodic exhumation history involving slow cooling in the Late Cretaceous and early Cenozoic followed by an increased cooling rate in the early Eocene.

Overall Tectonic and Exhumation History

AFT and apatite (U-Th)/He studies from the four regions of the TAM indicate variable uplift and exhumation prior to a pervasive upheaval of the entire range in the early Cenozoic. AFT results show that exhumation of the TAM is episodic and that different fault blocks record variable block movement of different amounts at different times (Fitzgerald, 1992).

Review of fission-track studies of the TAM indicate initiation of consistent exhumation affecting all of the TAM in the early Cenozoic, ranging from 45–55 Ma depending on the region. Additionally, the central TAM and Scott Glacier region were affected by Cretaceous exhumation. Therefore, to interpret the tectonic development and exhumation history of the TAM overall, no one sampling profile is indicative of the complete exhumation history nor can the exhumation history of the TAM be assumed to be uniform throughout. Profiles are variable with respect to the amount of exhumation recorded at each locality, particularly for the Late Cretaceous event, but are very consistent with respect to the timing of exhumation episodes (Fitzgerald and Stump, 1997).

METHODS

Thermochronology

In order to assess exhumation history and possible differential movement of the TAM across Byrd Glacier, both thermochronological and geomorphological methods were used. Since (U-Th)/He thermochronology has emerged as an important tool for quantifying the cooling history of rocks as they pass through the upper 1 - 3 kilometer of the crust (Ehlers and Farley, 2003), this analytical method was utilized to accomplish the thermochronological objectives of this study. The single crystal (U-Th)/He dating methods are based on the production of ^{4}He nuclei (α particles) by uranium and thorium series as well as ^{147}Sm decay (Farley, 2002; Zeitler et al., 1987). The helium closure temperature for apatite is ~ 70 °C and for zircon is ~ 180 °C (Reiners and Farley, 2001; Reiners et al., 2002).

The measurement of helium in apatite and zircon therefore can be used to interpret the cooling history of rocks that have undergone exhumation. With complete He accumulation in apatite occurring at temperatures below 70 °C, this closure temperature is substantially lower than other thermochronometers, allowing apatite (U-Th)/He ages to document the latest stages of cooling in the uppermost crust (Ehlers and Farley, 2003). Therefore, apatite helium thermochronology was chosen to assess exhumation history and differential movement across Byrd Glacier. Zircon (U-Th)/He thermochronology was also utilized to complement the apatite data.

For the thermochronologic study, nine igneous and metamorphic rocks were collected at known elevations north and south of Byrd Glacier (Table 1). In order to extract apatites and zircons for analysis, standard crushing, magnetic, and heavy liquid separation procedures were carried out on rock samples. Separated grains were then hand-picked under a binocular microscope on the basis of morphology, size, clarity, euhedral crystal shape, and, in the case of apatite, lack of optically detectable inclusions (Figure 6). Separates were dated using standard apatite and zircon (U-Th)/He thermochronology laboratory procedures as explained in Appendix 1. This involved releasing helium by laser heating of apatites and zircons in an ASI Alphachron and spiking the gas with ^3He for $^4He/^3He$ analysis. Next, apatites and zircons were dissolved and solutions were analyzed for uranium and thorium with an Inductively Coupled Plasma Mass Spectrometer. Ages were then calculated with an iterative process using blank corrected helium, thorium, and uranium values.

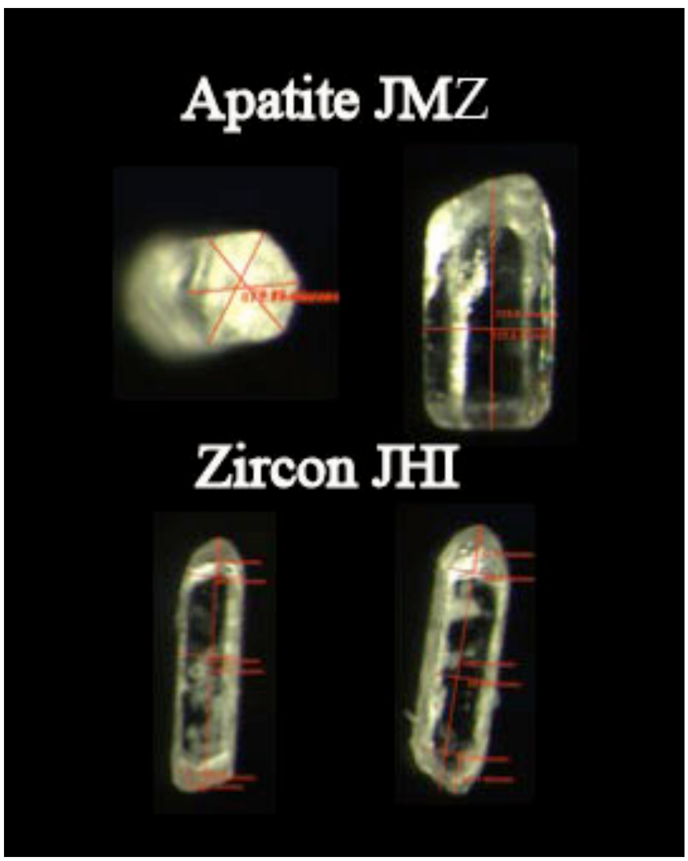

Figure 6. Apatite and zircon grains selected and measured for analysis.

Table 1

Rock sample data across Byrd Glacier. Elevations above sea level.

Sample Name	Rock Type	Glacier Side	Elev (m)	Elev Error +/- (m)
JID	Granite	North	600	50
JIF	Granite	North	1800	10
JIP	Gneiss	North	800	50
JMG	Granite	North	200	50
ESPR	Dolerite	North	3450	10
JHG	Tuff	South	1750	50
JHI	Quartzite	South	1700	50
JJW	Schist	South	100	50
JMZ	Granite	South	1150	50

Geomorphology

For assessing possible differential movement in this area from a geomorphological standpoint, the Kukri Peneplain was chosen as a datum. As this erosional surface becomes a structural datum likely at a relatively uniform elevation at the time of its formation, the objective was to determine its current elevation north and south of Byrd Glacier in order to quantify any displacement. To map the elevation of the Kukri Peneplain across Byrd Glacier, imagery from 30-meter resolution Landsat Image Mosaic of Antarctica (LIMA) was draped over 30-meter resolution Aster global Digital Elevation Model (DEM) of the region. These were processed in the Arc Geographic Information System programs, Arc Map, Arc Scene and Arc View. These data were then analyzed with Arc Scene and compared with on-site photos in order to visually identify the location of points along the Kukri Peneplain north and south of Byrd Glacier (Figure 7).

The locations of these points were then mapped in Arc Map on LIMA images and elevations were extracted from DEM data to estimate the elevation of the Kukri

Peneplain north and south of Byrd Glacier. After the points were identified, the distances between the points along the north and south sides were measured with reference to a linear transect through the long axis of Byrd Glacier. To more accurately compare the elevation of the Kukri Peneplain across Byrd Glacier, the dips of the north and south inferred trend lines were determined. The difference of the aligned points forming north and south trend lines were measured to assess the amount of offset.

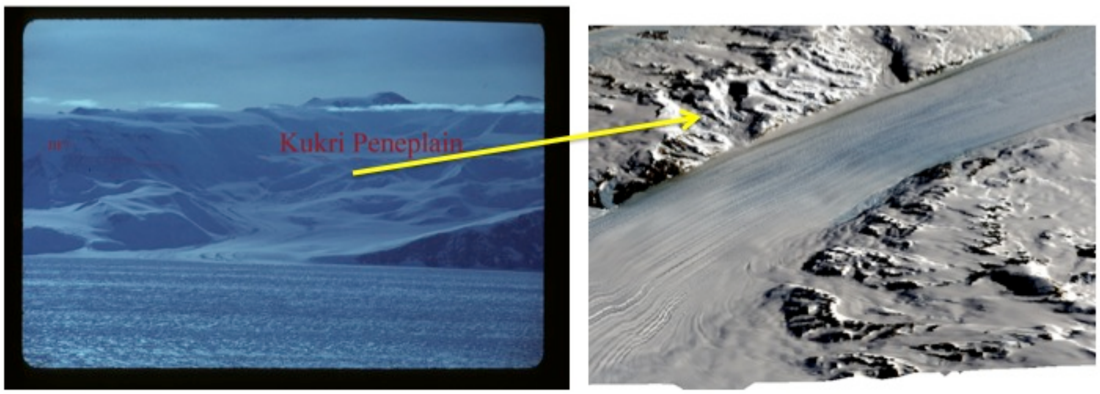

Figure 7. Comparison of on site photos of the Byrd Glacier region with combined Landsat image and DEM data to identify location and extract elevation of the Kukri Peneplain.

RESULTS

Thermochronology

The locations of the rock samples, are labeled in Figure 8. Apatite and zircon (U-Th)/He thermochronological analytical data from each sample are given in Table 2. To assess cooling histories and derive exhumation rates, age versus elevation data were plotted in Matlab utilizing the equations of York (1969) to compute a least-squares linear regression. In the regression analysis, the age variable was regressed taking into account two sigma (2σ) error uncertainties for each data point and mean squared weighted deviation (MSWD) values were derived.

The elevation of rocks ESPR and JIF are estimated to be accurate within 10 meters based on helicopter altimeter readings at the collecting sites. Elevations of the other rocks are based on mapping localities on the base map with a 200-meter contour interval and are estimated to be accurate within 50 meters. The mean age for the suite of apatites and zircons from each rock sample is listed along with 2σ errors. Additional information on apatite and zircon (U-Th)/He analytical data is included in Appendices 2 and 3 respectively.

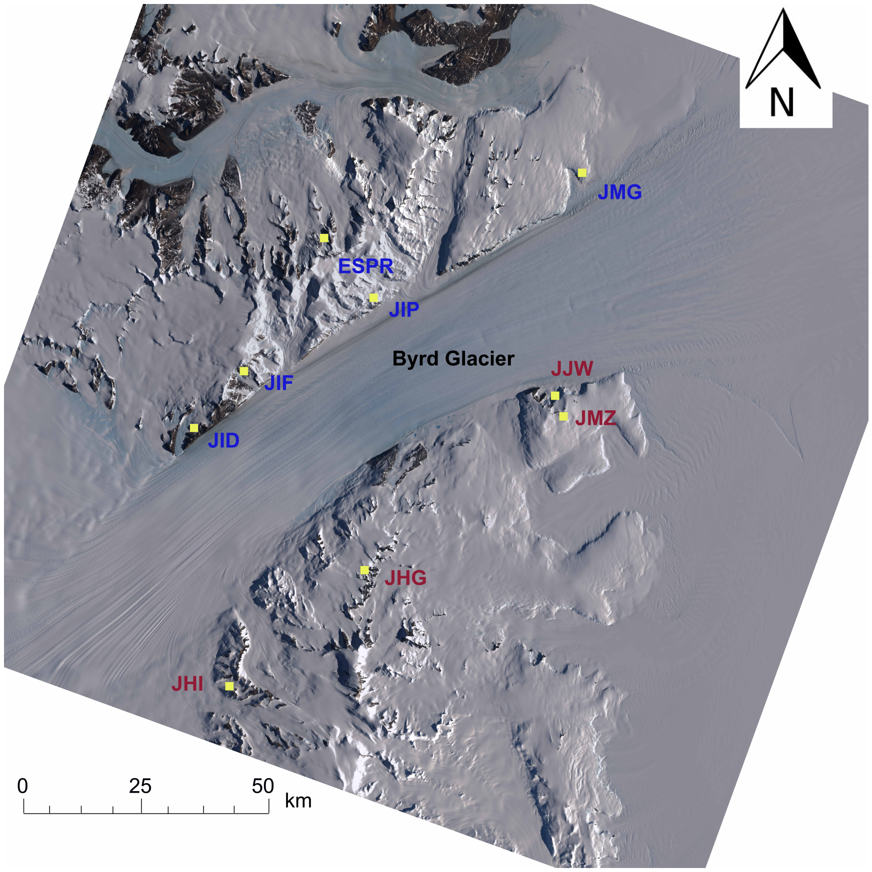

Figure 8. Rock sample locations north (in blue) and south (in red) of Byrd Glacier.

Table 2

Apatite and Zircon Data. Age with 2σ errors*. Elevation above sea level.*

Rock	Side	Elev. (m)	Elev. Error (m)	Ap. Mean Age (Ma)	Zr. Mean Age (Ma)
ESPR	North	3450	10	142.9 ± 17.5	177.9 ± 0.9
JIF	North	1800	10	102.1 ± 9.3	182.5 ± 11.5
JIP	North	800	50	52.8 ± 18.0	339.5 ± 103.4
JID	North	600	50	69.2 ± 18.2	52.9 ± 39.3
JMG	North	200	50	50.5 ± 6.8	100.5 ± 18.3
JHG	South	1750	50	54.2 ± 16.6	102.3 ± 21.3
JHI	South	1700	50	53.9 ± 19.2	64.8 ± 33.8
JMZ	South	1150	50	39.3 ± 14.5	80.0 ± 45.6
JJW	South	100	50	-	49.1 ± 6.6

Apatite. Eight out of the nine rock samples produced apatites of measurable quality providing analytical data from five rocks north of Byrd Glacier and three rocks south of Byrd Glacier. Sample JJW did not yield datable apatites. Results indicate apatite ages with 2σ error range from 142.87 ± 8.77 to 39.31± 5.93 Ma. All apatite data were plotted with age versus elevation displaying the MSWD (Figure 9). From the slope of the derived regression equation for all apatite data, the exhumation rate between ~ 140 – 40 Ma with 2σ error is 0.04 ± 0.01 mm/yr with an MSWD of 10.07.

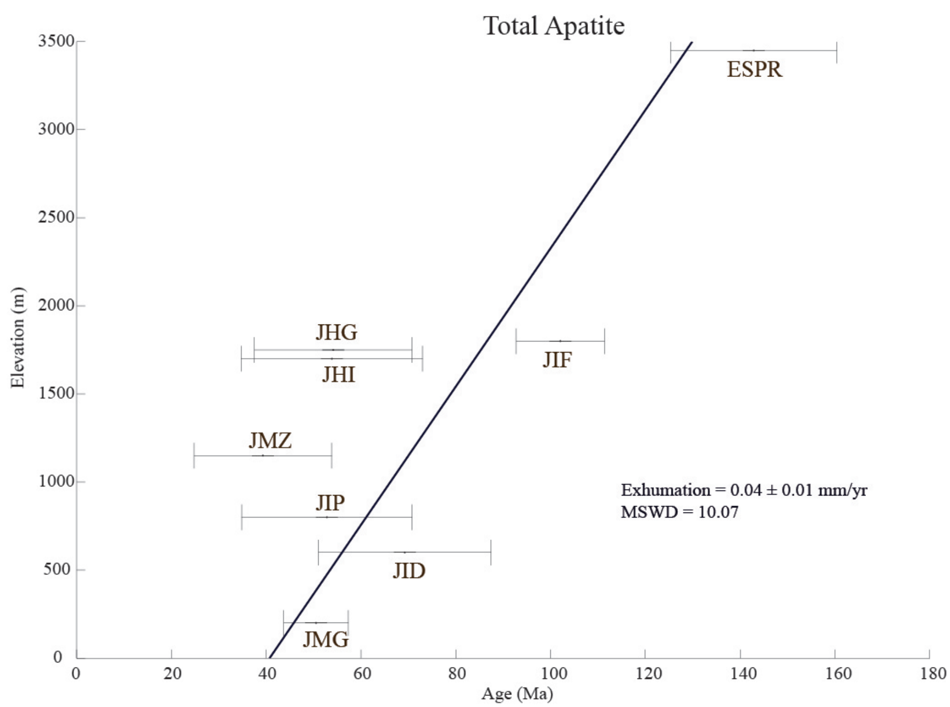

Figure 9. Total apatite age versus elevation plot. Bold line represents least squares regression. Black error bars represent 2σ. Elevation above sea level.

To further assess cooling histories and possible differential movement north and south of Byrd Glacier, apatite age versus elevation data were plotted separately north and south of Byrd Glacier and least squares regressions were determined. Analysis of apatite data north of Byrd Glacier with 2σ error reveals an exhumation rate of 0.03 ± 0.003 mm/yr between ~ 140 – 50 Ma with an MSWD of 1.5056 (Figure 10). Analysis of apatite data south of Byrd Glacier with 2σ error reveals an exhumation rate of 0.04 ± 0.03 mm/yr between ~ 55 - 40 Ma with an MSWD of 0.0056 (Figure 10). Separation of apatite age-versus-elevation data north and south of Byrd Glacier produces exhumation rates similar to that derived from the total sample set, but separating the samples leads to improved MSWD values.

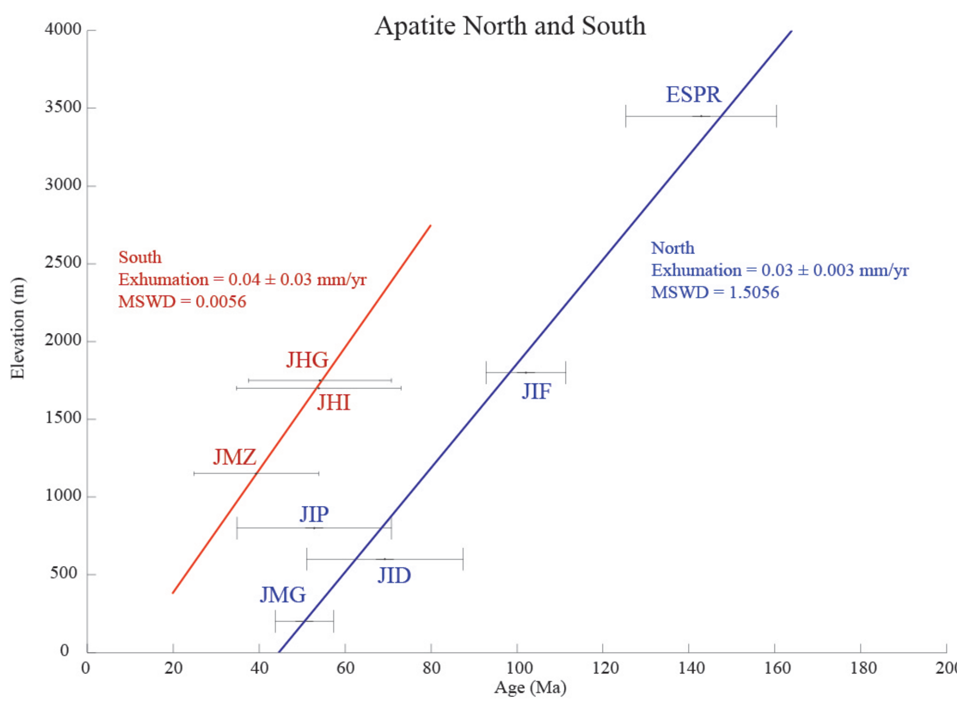

Figure 10. Apatite north and south of Byrd Glacier age versus elevation plot. Blue (north) and red (south) lines represent least squares regressions. Black error bars represent 2σ. Elevation above sea level.

Zircon. Eight out of the nine rock samples produced reasonable zircon data, four samples from north of Byrd Glacier and four from south (Table 2). The JIP zircon date of 339.47 Ma is excluded for several reasons. All JIP grains were significantly larger than zircon grains from other samples in this study. With the slow cooling rate as observed in the TAM, variables can exist where grains with different sizes can diffuse differently and produce cooling histories that are different (Reiners and Farley, 2001). Other possible related variables to affect the age interpretation are U-Th zoning (Hourigan et al., 2005), radiation damage (Nasdala et al., 2004), retention of He affected by experimental artifacts, and unknown uncertainties of He diffusion in zircon. Also, since the ages of all apatite and zircon samples except for JIP are less than ~ 180 Ma, the age of Ferrar magmatisim, it is unlikely that JIP was not affected as well by this thermal pulse.

Dates from the remaining eight zircon samples with 2σ error have an age range of 182.48 ± 8.16 to 49.08 ± 3.28 Ma. All zircon data were plotted with age versus elevation displaying MSWD values. From the slope of the regression equation, the exhumation rate between ~ 180 - 50 Ma with 2σ error for all zircon data with 2σ error is 0.03 ± 0.004 mm/yr with a MSWD of 26.45 (Figure 11). These data compare favorably with that of both the total and the separated apatite data.

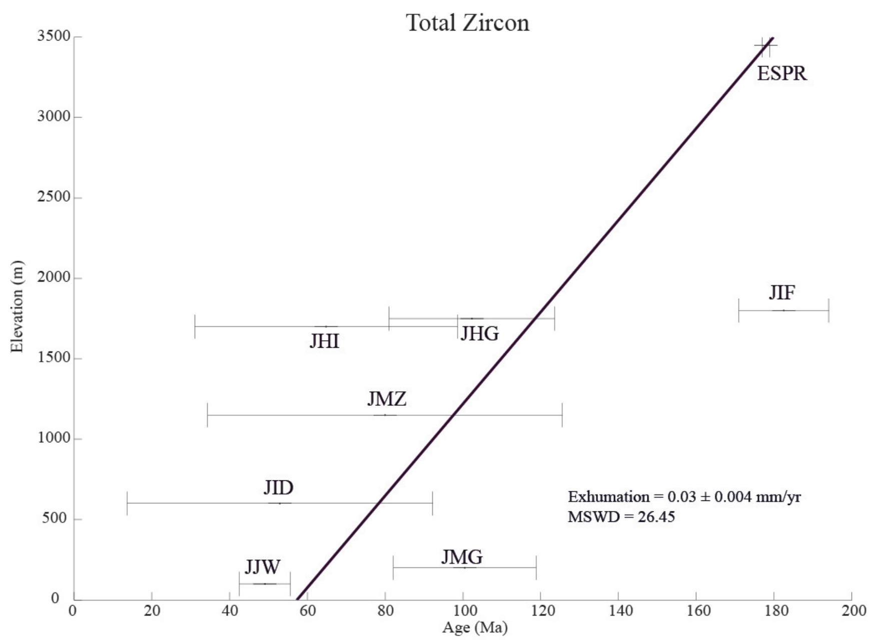

Figure 11. Total zircon age versus elevation plot. Bold line represents least squares regression. Black error bars represent 2σ. Elevation above sea level.

To further assess cooling histories and possible differential movement north and south of Byrd Glacier, zircon age versus elevation data were plotted separately north and south of Byrd Glacier and least squares regressions were determined. Analysis of zircon data north of Byrd Glacier with 2σ error reveals an exhumation rate of 0.06 ± 0.04 mm/yr between ~ 180 – 50 Ma with an MSWD of 26.45 (Figure 12). Analysis of zircon data south of Byrd Glacier with 2σ error reveals an exhumation rate of 0.04 ± 0.01 mm/yr between ~ 100 - 50 Ma with an MSWD of 1.65 (Figure 12). The south side rate of exhumation is only slightly higher than the total zircon rate, and is consistent with the derived rates of exhumation from apatite. The north side rate of exhumation at ~ 0.06 mm/yr is higher than the other derived rates by ~ 0.02 mm/yr. That the MSWD for this data set is high (26.45) casts doubts on the reliability of this rate.

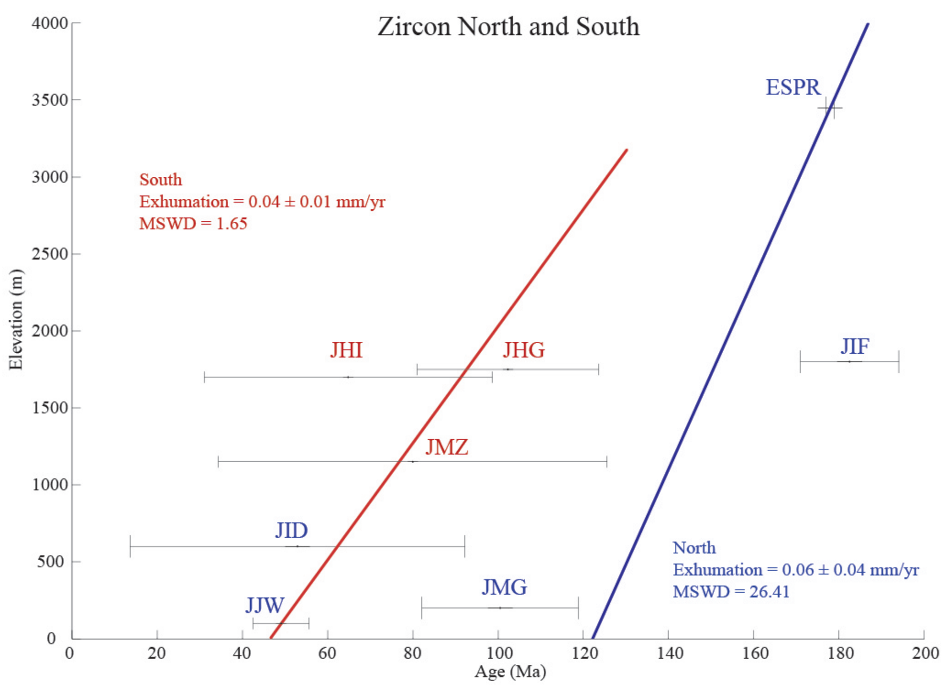

Figure 12. Zircon north and south of Byrd Glacier age versus elevation plot. Blue (north) and red (south) lines represent least squares regressions. Black error bars represent 2σ. Elevation above sea level.

Geomorphology

Based on field photographs, the Kukri Peneplain was located at seven points on Landsat imagery of the area, four points on the north side of Byrd Glacier and three points on the south side as shown in Figure 13. From these locations, elevations were extracted from the DEM revealing that the observed Kukri Peneplain points are at higher elevations on the south side relative to the north (Table 3). Orthogonal projections of these points were then made onto a transect parallel to Byrd Glacier. The distances between points on transect A – A' are measured from the southwesternmost point (Figure 13, Table 3). Both north and south points show elevations higher in the east closer to the coast indicating a trend of slight dip to the west.

The elevation points and distance from A along transect A – A' (Figure 13) of the Kukri Peneplain were plotted on a distance versus elevation diagram as a pair of cross sections north and south of Byrd Glacier in Figure 14. In order to more accurately compare the elevation of the projected peneplain across Byrd Glacier, the dips were calculated. The results are west dips of 1.79^{o} on the north side and 1.81^{o} on the south side of Byrd Glacier.

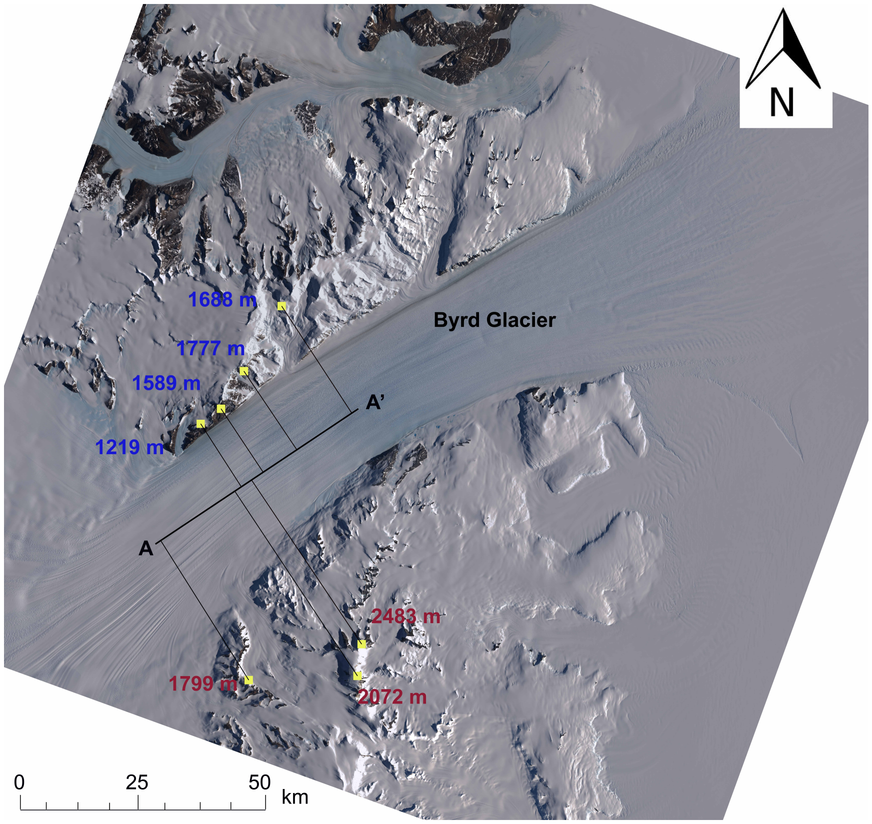

Figure 13. Kukri Peneplain locations with corresponding elevations plotted on Byrd Glacier DEM overlain with Landsat image. Distance between points measured with respect to A – A' transect. Elevations above sea level.

Table 3

Kukri Peneplain elevation and distance across Byrd Glacier along A –A' transect. Elevations above sea level.

N Dist. (m)	N Elev. (m)	S Dist. (m)	S Elev. (m)
20677	1219	0	1799
27404	1589	17671	2072
33679	1777	22767	2483
45087	1688		

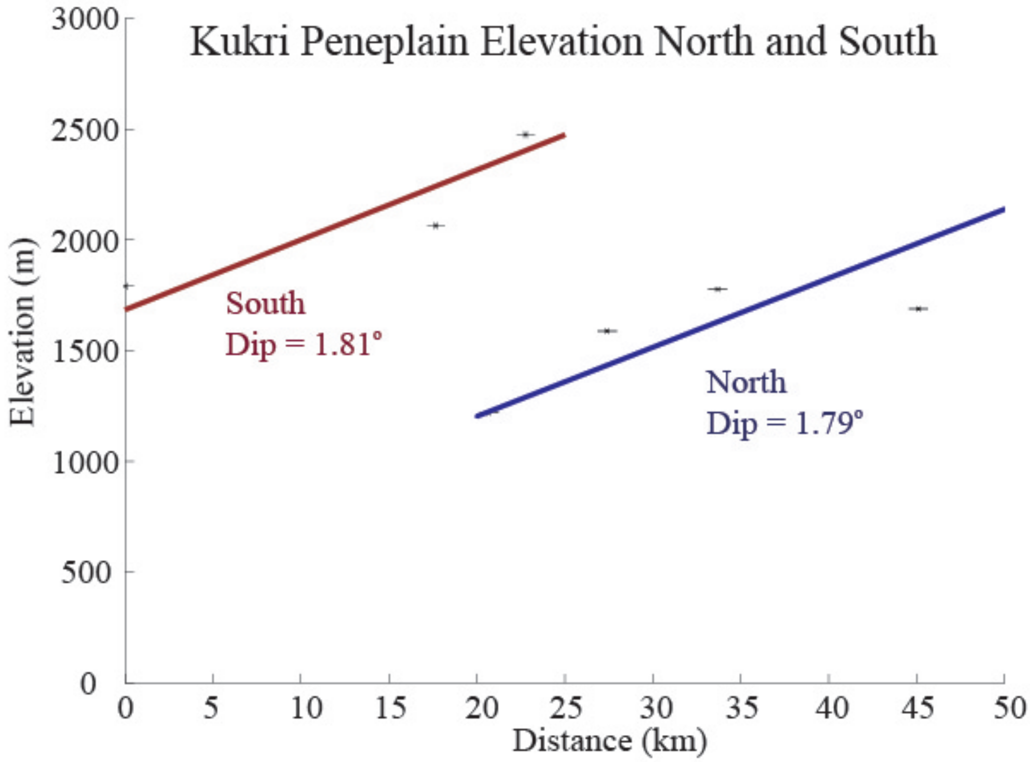

Figure 14. Kukri Peneplain distance versus elevation plotted as a pair of cross sections across Byrd Glacier. Bold lines represent north (blue) and south (red) least square regressions. Elevation above sea level.

DISCUSSION

Thermochronology

When comparing both apatite and zircon data across Byrd Glacier, plots reveal that at similar elevations southern ages are younger than northern ages and at similar ages southern elevations are higher than northern elevations (Figures 10 and 12). This indicates differential movement across Byrd Glacier. Two models could plausibly explain this inferred differential movement. In the first model, a relatively uniform exhumation across Byrd Glacier is followed by later fault displacement. The second model involves differential exhumation with the south side exhumed at a more rapid rate than the north side. In order to test the relative merits of these models, exhumation rates from apatite and zircon data north and south of Byrd Glacier were compared.

The exhumation rates inferred from apatite data across Byrd Glacier are identical within error, 0.03 ± 0.003 mm/yr to the north and 0.04 ± 0.03 mm/yr to the south. The exhumation rate of 0.04 ± 0.01 mm/yr derived from zircon data from the south side of Byrd Glacier is also similar to the apatite rates. The exhumation rate of 0.06 ± 0.04 mm/yr from the north-side zircon data is somewhat higher. With the exception of the north side zircon data, the exhumation rates across Byrd Glacier are comparable, suggesting that the differential movement was more likely attributable to an offset from fault displacement. In order to quantify the offset across Byrd Glacier apatite and zircon offset data with 2σ error were compared.

Apatite. North and south apatite (U-Th)/He data reveal similar yet offset cooling histories that suggest differential movement across Byrd Glacier. To quantify offset, regression equations from apatite age versus elevations plots north and south of Byrd

Glacier were compared to calculate the difference in elevation (Figure 15). The regression equations of y = 33.52x – 1494 and y = 40.82x – 476 north and south of Byrd Glacier with y representing elevation and x representing age were utilized in calculations. Offset was calculated by inputting an age value x as the predictor variable into each regression equation resulting in a predicted elevation value for a given age. Then the north side elevation was subtracted from the south to determine the difference in elevation of the inferred rock at the same age across Byrd Glacier. The apatite data across Byrd Glacier is well constrained for comparison in the range of ~ 40 – 60 Ma as rocks in this age range are represented in both north and south data. Therefore an age value of 50 Ma was used for x in both north and south regression equations. The resulting elevation difference across Byrd Glacier with 2σ error is 1379 ± 159 meters.

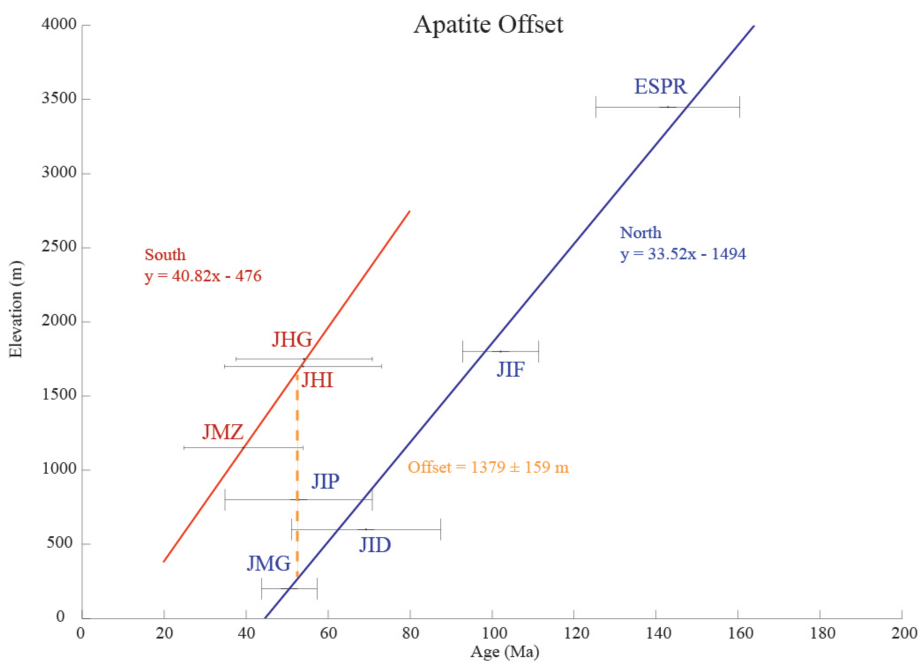

Figure 15. Offset calculated from apatite regression equations north and south of Byrd Glacier from age versus elevation plot. Blue (north) and red (south) lines represent least squares regressions. Black error bars represent 2σ. Elevation above sea level.

Zircon. Zircon (U-Th)/He data reveal similar cooling histories across Byrd Glacier that suggest differential movement. To quantify offset, regression equations from zircon age versus elevations plots north and south of Byrd Glacier were derived to calculate the difference in elevation (Figure 16). The regression equations of $y = 61.83x - 7754$ and $y = 37.95x - 1763$ north and south of Byrd Glacier with y representing elevation and x representing age were utilized in calculations. Offset was calculated by inputting an age value x as the predictor variable into each regression equation resulting in a predicted elevation value for a given age. Then the south side elevation was subtracted from the north to determine the difference in elevation of inferred rock at the same age across Byrd Glacier. The zircon data across Byrd Glacier is well constrained for comparison in the range of ~ 50 – 100 Ma as rocks in this age range are represented in both north and south data. Therefore an age value of 75 Ma was used for x in both north and south regression equations. The resulting elevation difference across Byrd Glacier with 2σ error is 4000 ± 3466 meters.

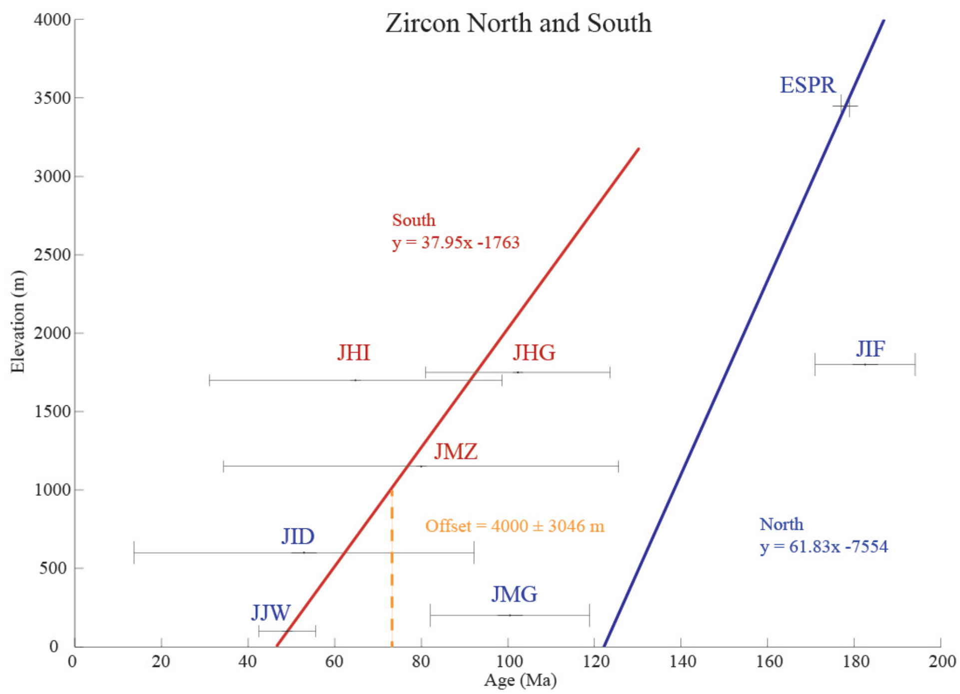

Figure 16. Offset calculated from zircon regression equations north and south of Byrd Glacier from age versus elevation plot. Blue (north) and red (south) lines represent least squares regressions. Black error bars represent 2σ. Elevation above sea level.

Geomorphology

To assess differential movement from a geomorphologic perspective and to complement thermochronologic data, the Kukri Peneplain was projected as a pair of planar surfaces across Byrd Glacier (Figure 17). As the peneplain dips differ only by 0.03°, where they overlap the transect A – A' (Figure 13), the elevation of the peneplain across Byrd Glacier can be compared. However, this does involve the uncertainties of assuming the peneplain has consistent strikes across Byrd Glacier and is not significantly deformed. The strikes could not be assessed in this study, as locations of the Kukri Peneplain could not be extended farther north and south of the measured points due to limited visible exposure and no available on-site data.

To measure the offset of the Kukri Peneplain, the elevation difference was calculated across Byrd Glacier by comparing the peneplain elevations on either side at a point where the traces of the peneplain overlapped (Figure 18). The regression equations from Kukri Peneplain distance versus elevation least squares regression plots revealed $y = 0.0312x + 578$ and $y = 0.0316x + 1692$ north and south of Byrd Glacier with y representing elevation and x representing distance. Elevations were calculated based on an x value of distance as the predictor. The north side elevation was subtracted from the south side to determine the difference in elevation of the peneplain at the overlapping point on the A – A' transect. The peneplain elevation data across Byrd Glacier overlaps along the A – A' transect between ~ 20.7 – 22.7 kilometers (Figure 13). Therefore a distance value of 21.7 kilometers was chosen. The calculated difference in elevation of the Kukri Peneplain across Byrd Glacier with 2σ error is 1122 ± 4.7 meters.

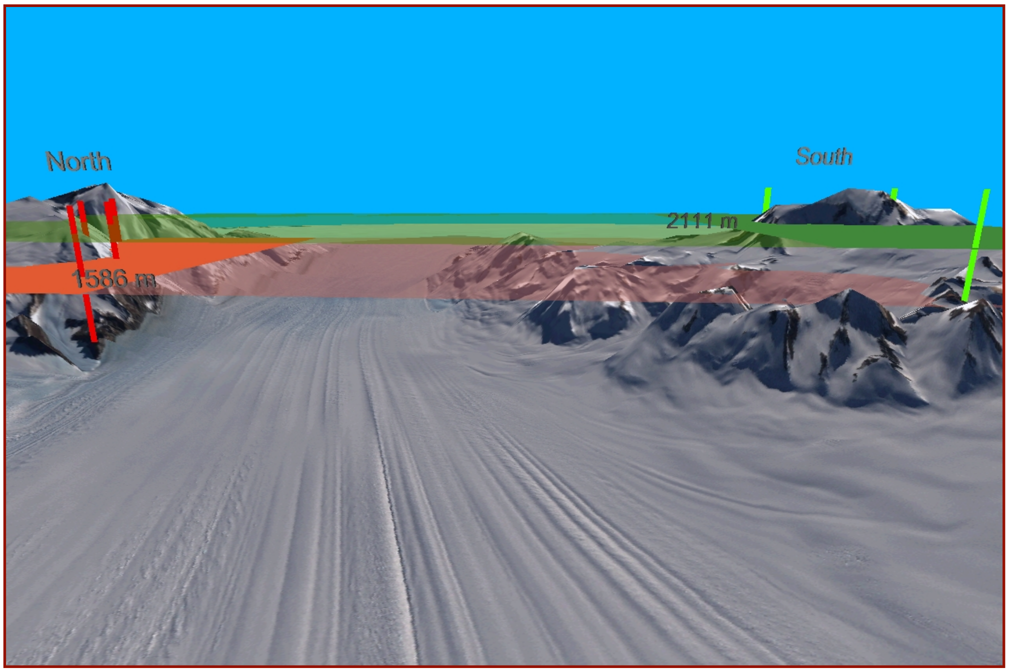

Figure 17. Kukri Peneplain projected as planar surfaces north and south of Byrd Glacier to assess offset.

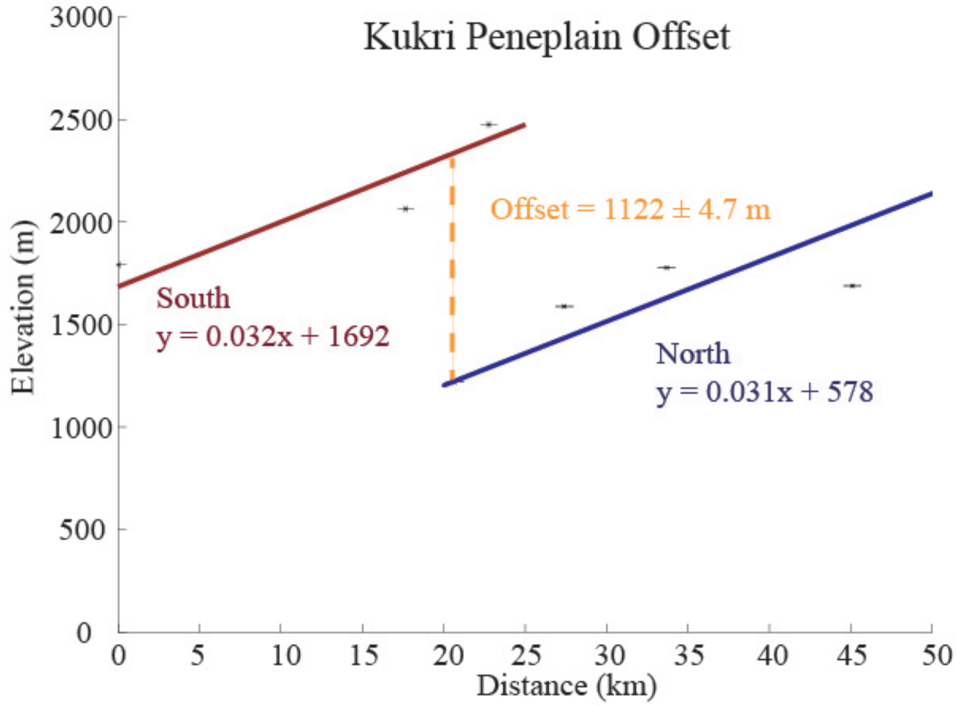

Figure 18. Offset calculated from Kukri Peneplain regression equations across Byrd Glacier from distance versus elevation plot. Blue (north) and Red (south) lines represent least squares regressions. Black error bars represent 2σ. Elevation above sea level.

Comparison of Thermochronologic and Geomorphologic Results

Both thermochronologic and geomorphologic data results indicate the south side of Byrd Glacier was displaced relative to the north side. A comparison of offset as indicated by apatite thermochronological and geomorphologic data reveals a close correspondence in the amount of vertical differential movement with 2σ error, 1379 ± 159 meters versus 1122 ± 4.7 meters respectively. The zircon data with 2σ error indicating an offset of 4000 ± 3466 meters is somewhat greater than that indicated by the other techniques. However with the high uncertainties taken into account, it is within 2σ error range of apatite and geomorphologic data. This higher uncertainty may be explained by the larger MSWD value for the regression line fitted to these data.

CONCLUSION

The results of this study suggest a model of relatively uniform exhumation followed by fault displacement that uplifted the south side of Byrd Glacier relative to the north side. The thermochronologic and geomorphologic data of this study suggest that the timing of the fault displacement occurred sometime after ~ 40 Ma. More extensive geologic mapping and analysis of the Byrd Glacier region could help to better constrain the location of the fault and timing of the displacement.

This method of combining thermochronologic and remote geomorphologic analysis utilizing a peneplain as a datum, has provided a better understanding of the differential movement and denudation history of the Byrd Glacier region. The results of this study can complement and fill in gaps in the knowledge of tectonic development and landscape evolution of Antarctica. Also the methodology of this study can be utilized in comparison with thermochronologic and geomorphologic studies elsewhere within the TAM.

REFERENCES

Ehlers, T.A., and Farley, K.A. (2003). Apatite (U–Th)/He thermochronometry: methods and applications to problems in tectonic and surface processes, *Earth and Planetary Science Letters, 206*, 1–14.

England, P., and Molnar, P. (1990). Surface uplift, uplift of rocks, and exhumation of rocks. *Geology*, *18*, 1173-1177.

Farley, K.A. (2002). (U-Th)/He dating: techniques, calibrations, and applications. *Noble Gas Geochemistry, Reviews in Mineralogy and Geochemistry*, *47*, 819–843.

Fitzgerald, P.G., and Gleadow, A.J.W. (1988). Fission-track geochronology, tectonics and structure of the transantarctic mountains in Northern Victoria land, Antarctica. *Chemical Geology*: *Isotope Geoscience*, 73, Issue 2, 169-198.

Fitzgerald, P.G. (1992). The Transantarctic Mountains of southern Victoria Land: The application of apatite fission track analysis to a rift shoulder uplift. *Tectonics*, vol. 11, no. 3, 634-662.

Fitzgerald, P.G. (1994). Thermochronologic constraints on post-Paleozoic tectonic evolution of the central Transantarctic Mountains, Antarctica. *Tectonics*, vol. 13, no. 4, 818-836.

Fitzgerald, P.G., and Stump, E. (1997). Cretaceous and Cenozoic episodic denudation of the Transantarctic Mountains, Antarctica: New constraints from apatite fission track thermochronology in the Scott Glacier region. *Journal of Geophysical Research*, vol. 102, no. B4, 7747-7765.

Fitzgerald, P. G., Baldwin, S.L., Webb, L.E., O'Sullivan, P.B. (2006). Interpretation of (U-Th)/He single grain ages from slowly cooled crustal terranes: a case study from the Transantarctic Mountains of southern Victoria Land. *Chemical Geology*, *225*, (1–2), 91–120, doi:10.1016/j.chemgeo.2005.09.001.

Fleming, T.H., Heimann, A., Foland, K.A., Elliot, D.H. (1997). $^{40}Ar/^{39}Ar$ geochronology of Ferrar Dolerite sills from the Transantarctic Mountains, Antarctica: Implications for the age and origin of the Ferrar magmatic province. *Geological Society of America Bulletin, 109, p. 533-546,* doi:10.1130/0016-7606.

Gleadow, A.J.W., and Fitzgerald, P.G. (1987). Uplift history and structure of the Transantarctic Mountains: new evidence from fission track dating of basement apatites in the Dry Valleys area, southern Victoria Land. *Earth and Planetary Science Letters*, *82*, Issue 1-2, 1-14.

Grindley, G.W., and Laird, M.G., (1969). Geology of the Shackleton coast: Antarctic Map Folio Series, Folio 12, XIV, New York, *American Geographical Society.*

Hourigan, J.K., P.W., Brandon, M.T. (2005). U–Th zonation dependent alpha-ejection correction in (U–Th)/He chronometry. *Geochim. Cosmochim. Acta, 69,* 3349–3365.

Nasdala, L., Reiners, P.W., Garver, J.I., Kennedy, A.K., Stern, R.A., Balan, E., Wirth, R. (2004). Incomplete retention of radiation damage in zircon from Sri Lanka. *American Mineral, 89*, 219–231.

Reiners, P. W. and Farley, K. A. (2001) Influence of crystal size on apatite (U-Th)/He thermochronology: an example from the Bighorn Mountains, Wyoming. Earth and Planetary Science Letters vol. 188 (3-4) pp. 413-420.

Reiners, P. W., Farley, K. A. and Hickes, H. J. (2002) He diffusion and (U-Th)/He thermochronometry of zircon: initial results from Fish Canyon Tuff and Gold Butte. Tectonophysics vol. 349, pp. 297-308.

Stump, E., and Fitzgerald, P.G. (1992). Episodic uplift of the Transantarctic Mountains. *Geology*, *20*, no. 2, 161-164.

York, D. (1969) Least-squares fitting of a straight line, *Can. J. Phys.* 44.

Zeitler, P.K., Herczig, A.L., McDougall, I., Honda, M. (1987) U-Th-He dating of apatite: a potential thermochronometer. *Geochim Cosmochim Acta*. *51*, 2865-2868.

APPENDIX I

ASU (U/TH)/HE THERMOCHRONOLOGY METHODS

Heavy mineral separates are prepared using standard crushing, magnetic, and heavy liquid separation methods. From these separates apatite and zircon grains were hand picked, based on size, clarity, euhedral crystal shape and, in the case of apatite lack of optically detectable inclusions using a Leica MZ16 binocular microscope with 184x magnification equipped with a video camera and capable of dark-field illumination. When available, inclusion free zircons were also selected, but it was not always possible to find 5 optically inclusion-free zircons. This appears to have little or no adverse affects when compared to the effects that inclusions have on apatites. The camera takes digital still pictures that are processed on a Dell computer using the Image Pro software package to measure the crystal dimensions that are used to correct the (U-Th)/He age of the crystal for He loss due to a recoil. To make sure the measurements obtained from the digital pictures are correct, each magnification setting of the microscope and the camera itself are calibrated using a traceable NIST dimension standard on a yearly basis.

If present titanite grains are also picked, usually with sub- to anhedral shape, but in large enough size to abrade away the outer 20-30 microns, so that an a-ejection correction does not have to be carried out. Between 15-30 shards of titanite are put in a stainless steel abrader with a very small amount of similarly sized pyrite that serves as an abrasive. Abraders are fed with 10psi compressed air and typically are run overnight to attain grains sufficiently abraded that they can be analyzed. The level of abrasion is checked by microscopic examination of the size of the abraded grains.

After determination of the dimensions or after abrasion each selected grain is loaded into 0.027" OD x 0.04" long Nb tubes. Tubes are then loaded into a 25 spot stainless steel sample-holder of an ASI Alphachron (U-Th)/He dating system ('mini-He'), with 2 blank tubes, and 3 tubes loaded with a shard of Durango apatite age standard for apatite samples, a combination of Durango apatite and Fish Canyon zircon age standards for zircon samples, and 3 tubes loaded with abraded Fish Canyon titanite age standards for titanites, and then pumped down overnight. Helium is released from apatite by laser heating with a 980nm diode laser for 5 minutes at 11 Amps, and from zircon and titanite by laser heating for 10 minutes at 15 Amps. The gas is spiked with ^{3}He and exposed to a hot SAES NP-10 getter for 2 minutes, after which the gas is expanded into a Pfeiffer – Balzers Prisma Quadrupole with a range of 0-100 amu, Channeltron electron multiplier and a faraday detector that also has a room temperature SAES NP-10 getter in the vacuum chamber. The ASI Alphachron does not have a He cryogenic refrigerator to concentrate the sample gas before inlet into the quadrupole mass spectrometer as the volume of the extraction line is so small that the gain in volume and gas let into the mass spectrometer chamber would be minimal.

Helium blanks are determined by heating Nb tubes following apatite, titanite, and zircon procedures. The long-term average for the blanks is 0.036 ± 0.010 femto-mole for all procedures.

To analyze the ^{4}He/^{3}He composition of the gas, four masses are monitored during analysis: Mass 1 as a proxy for HD contributions to the Mass 3 peak, Mass 3 for ^{3}He, Mass 4 for ^{4}He and Mass 5 for the background. The HD contribution to the ^3He peak ranges from 0.035 to 0.040% for apatite analyses and 0.045 to 0.055% for zircon/titanite analyses. ^4He concentrations were calculated by comparing the sample $^4He/^3He$ to a set of standard analyses run prior to and after the sample analysis. Short-term (5-10 standard analyses) reproducibility is on the order of 0.03-0.05%, while the long-term (complete sample holder run) reproducibility is on the order of 0.05-0.08%. The composition of the ^4He standard gas tank is known to 1.2%, which represents the largest contribution to the error in this part of the analytical process.

After initial He extraction all samples were re-extracted with the same analytical procedure. In all cases apatite and in most cases titanite grains re-extracted perfectly to blank levels, while zircons and some titanites were re-extracted until helium yields were less than 0.5% of the originally extracted gas. On occasion this required multiple re-extractions, the reasons for this phenomenon are poorly understood, but it appears to not negatively affect the final calculated age (e.g. Reiners, 2005).

Following He measurement the Nb tubes containing the grains are unloaded and digested for U and Th analysis on an Inductively Coupled Plasma-Mass Spectrometer (ICP-MS). Given the characteristics of apatite vs. zircon and titanite the digestion procedures are very different. Apatite is dissolved in concentrated HNO_3 (Evans 2005), while zircon and titanite require the use of concentrated HF, HNO_3, and HCl combined with higher than ambient temperature and pressures (Reiners et al 2002, Reiners 2005). Due to this process, the tube containing the zircon/titanite also is dissolved. This precludes the use of Pt tubes as 'microcrucibles' for the helium extraction as the large amounts of Pt in solution would cause severe PtAr interferences on the U mass spectrum in the ICP-MS. This is the reason Nb microcrucibles are used. Nb has a high melting point so it does not melt during laser heating and it has a low atomic mass, which means that NbAr complexes do not cause interferences on the U mass spectrum.

Nb packages containing the apatites were transferred to 1.5 ml polypropylene microvials and a 25 µl microliter. A ^{235}U and ^{230}Th spike solution aliquot made up in 50% distilled ultra pure HNO_3 was added. The ^{235}U and ^{230}Th spike solution has a concentration of 15ng/ml and 5ng/ml respectively. Samples were then sonicated for 15 minutes and rested for 4 hours to allow for apatite dissolution. After this the samples were diluted with 375 µl of MilliQ 18.2 MegaOhm polished water to make up the final solution for analysis.

Zircon and titanite samples were dissolved following general procedures described by Reiners (2005). The Nb tubes containing the extracted samples were transferred into Teflon microvials (0.50 ml) and 50 µl of the same spike used for the apatite analysis was added together with 300 µl of distilled ultra pure concentrated HF. The vials were then put in the Teflon liners of large 125 ml Parr digestion vessels which each will hold a total of 10 vials. For pressure balance 10 ml of trace-metal-grade, concentrated HF and 0.45 ml trace metal grade concentrated HNO_3 are added to the liner. The digestion vessels were heated at 225˚C for 72 hours after which the samples are heated to dryness at low (60-75˚C) heat. When the samples are dry they are put back in the Parr digestion vessels, but now with 300 µl of distilled ultra pure concentrated HCl added to each vial, and 9 ml of trace metal grade concentrated HCl added to the liner and heated at 200˚C for 24 hours. Following this, samples are again heated to dryness before adding 12.5 µl of distilled ultra pure concentrated HF and 100 µl of distilled ultra pure concentrated HNO_3. The sample vials are closed and gently heated on a hot plate at 60-70˚ C for 30 minutes, before the contents are transferred to larger 15 ml polypropylene vials holding 1.5 ml of MilliQ 18.2 MegaOhm polished water to make up the final solution of 0.8% HF and 6% HNO_3 that is ready for analysis.

The solutions were analyzed on a Thermo X series quadrupole ICP-MS in the W.M. Keck Foundation Laboratory for Environmental Geochemistry at Arizona State University (ASU), using a micronebulizer with an uptake rate of 100 µl/minute. The analytical procedure consists of 7 and 10 cycles for apatite and zircon/titanite solutions respectively, in each cycle 150 sweeps of the following isotopes were conducted: ^{230}Th, ^{232}Th, ^{235}U, ^{238}U and ^{234}U, which can be used as a proxy for detection of isobaric interferences on the U mass spectrum for platinum-argides. During apatite analyses ^{147}Sm, ^{152}Sm, and ^{154}Sm were also analyzed to determine if any of the apatites have high enough Sm contents to have a significant effect on the calculated age. Since there is no Sm isotope in the spike actual Sm abundances in the solution are not calculagted.

Analyses are standardized by analyzing a spiked standard (SPST) solution, which is a mixture of the same spike solution used for the apatite and zircon solutions and a U and Th standard of known concentration. For SPST solutions run with the apatite samples 25 µl of spike is added to 25µl of the standard solution, which has a concentration of 25ng/ml of U and Th in 4% HNO_3, which is then diluted with 350 µl MilliQ 18.2 MegaOhm polished water to make the final solution. For zircons, 50 µl of spike is mixed with 50 µl of the standard solution to which 100 µl of distilled ultra pure concentrated HNO_3 and 12.5 µl of distilled ultra pure concentrated HF is added after which the solution is diluted with 1.5 ml of MilliQ 18.2 MegaOhm polished water to make up the final solution of 0.8% HF and 4-6% HNO_3 that is ready for analysis. One SPST solution is also added to each Parr digestion vessel to monitor for any effects of contamination during the Parr digestion process. So far we have not encountered any major differences between the SPST solutions that have gone through the Parr digestion process and those that are prepared without going through that process. Reproducibility of the spiked standard analysis is on the order of 0.75% for U and 0.85% for Th.

Total process blanks were determined by taking the empty Nb tubes used to determine the He blanks and by processing them with the samples through the preparation steps for U and Th analysis. Average Nb tube blanks for the apatite procedure are 0.53 ± 0.03 pg (1s standard error) U and 0.43 ± 0.04 pg (1s standard error) Th, while average Nb tube blanks are higher at 2.6 ± 0.3 pg (1 sigma standard error) U and 2.4 ± 0.7 pg Th (1 sigma standard error), reflecting the fact that the tube is totally dissolved.

Ages are calculated with an iterative process using blank corrected He, Th, and U values. Raw ages were corrected for a-ejection effects following methods described in Farley et al. (1996) and Farley (2002) for apatite and described by Hourigan et al. (2005) and Reiners (2005) for zircon. Due to the abrading, no a-ejection correction needs to be applied to the titanite ages. The long-term average age determined for Durango apatite in the NG^3L is 31.78 ± 1.25 (1s SD) Ma with a standard error of 0.07 Ma (n=328), the equivalent weighted average age calculated with ISOPLOT (Ludwig, 2008 – no rejections allowed) is 31.63 ± 0.15 (95% confidence, MSWD 5.8) Ma. and for Fish Canyon zircon it is 28.02 ± 1.54 (1s SD) Ma with a standard error of 0.21 Ma (n = 52). Analytical errors were propagated throughout the process and amount to 1.5 – 2.5% (1s). Errors associated with the a-ejection correction were not directly determined, but following discussions in, for example, Farley et al. (1996), Spotila et al. (1998), Hourigan et al. (2005), they are estimated to push the total error for the method to 3-4% (1s). The a-ejection corrections were made assuming a homogeneous U and Th distribution, which, especially for zircon, may often not be fully realistic and can account for significant added scatter in the age data (e.g. Hourigan et al. 2005).

REFERENCES

Evans, N. J., Byrne, J. P., Keegan, J. T., & Dotter, L. E. (2005) Determination of uranium and thorium in zircon, apatite, and fluorite: Application to laser (U-Th)/He thermochronology. Journal of Analytical Chemistry, vol. 60, no. 12, pp. 1159-1165.

Farley, K. A., Wolf, R. A., and Silver, L. T. (1996) The effects of long alpha-stopping distances on (U-Th)/He ages. Geochimica et Cosmochimica Acta, vol. 60, no. 21, pp. 4223-4229.

Farley, K. A. (2002) (U-Th)/He dating: techniques, calibrations, and applications. In: Noble Gases in geochemistry and cosmochemistry. Reviews in mineralogy and geochemistry vol. 47. Eds: Porcelli, D., Ballentine, C. J., and Wieler, R. The mineralogical society of America, Washington D.C., pp. 819-844.

Hourigan, J. K., Reiners, P. W., and Brandon, M. T. (2005) U-Th zonation-dependent alpha-ejection in (U-Th)/He chronometry. Geochimica et Cosmochimica Acta vol. 69, no. 13, pp. 3349-3365.

Ludwig, K.R. (2008) User's manual for Isoplot 3.70: A geochronological toolkit for microsoft excel: Berkeley Geochronological Center Special Publication 4, 77.

Reiners, P. W. and Farley, K. A. (2001) Influence of crystal size on apatite (U-Th)/He thermochronology: an example from the Bighorn Mountains, Wyoming. Earth and Planetary Science Letters vol. 188 (3-4) pp. 413-420.

Reiners, P. W., Farley, K. A. and Hickes, H. J. (2002) He diffusion and (U-Th)/He thermochronometry of zircon: initial results from Fish Canyon Tuff and Gold Butte. Tectonophysics vol. 349, pp. 297-308.

Reiners, P. W. (2005) Zircon (U-Th)/He thermochronometry. In: Low-temperature thermochronology: Techniques, interpretations, and applications. Reviews in mineralogy and geochemistry vol. 58. Eds: Reiners, P.W. and Ehlers, T. A. The mineralogical society of America, Washington D.C., pp. 151-179.

Spotila, J. A., Farley, K. A., and Sich, K. (1998) Uplift and erosion of the San Bernardino Mountains associated with transpression along the San Andreas fault, California, as constrained by radiogenic helium thermochronometry. Tectonics vol. 17, no. 3, pp. 360-378.

APPENDIX II

APATITE (U-TH)/HE DATA

#	Sample	Elevation	[^{4}He]	[^{238}U]	[^{232}Th]	Raw Age	1σ	% 1σ	R	L	$^{238}UF_T$	$^{232}ThF_T$	Mean F_T	Age $F_{T\,corr}$	1σ	2σ	[eU]	Th/U	1s	Mean Age	1 SD	2 SD
58		m	ncm^3	ng	ng	Ma	Ma		μm	μm				Ma	Ma	Ma	ppm			Ma	Ma	Ma
																			Apatite			
																			Zircon			
2176	ESPR a001	3450	0.5262	0.0271	0.0680	99.70	2.32	2.33	42.0	137.0	0.68	0.63	0.659	151.39	3.52	7.05	21.6	2.559	0.098			
2298	ESPR a003	3450	0.4006	0.0227	0.0577	90.32	1.47	1.62	49.0	87.3	0.67	0.63	0.657	137.52	2.23	4.47	20.9	2.594	0.055			
2300	ESPR a004	3450	0.2236	0.0140	0.0365	81.00	1.67	2.06	36.5	109.6	0.63	0.58	0.607	133.41	2.75	5.50	18.7	2.666	0.084			
2302	ESPR a005	3450	0.3159	0.0328	0.0471	58.89	1.14	1.94	44.7	101.6	0.67	0.62	0.656	89.74	1.74	3.48	26.1	1.462	0.039			
2306	ESPR a006	3450	0.3202	0.0167	0.0510	91.00	1.68	1.85	37.0	111.0	0.63	0.58	0.610	149.18	2.76	5.51	22.9	3.104	0.080	142.9	8.8	17.5
2201	JIF a004	1800	2.4477	0.2189	0.2049	74.89	1.31	1.75			0.75	0.72	0.746	100.37	1.75	3.51	55.3	0.953	0.021			
2227	**JIF a008**	**1800**	5.9151	0.6184	0.2244	72.00	1.30	1.81	38.1	198.2	0.79	0.76	0.783	92.01	1.67	3.33	78.4	0.370	0.009			
2292	**JIF a010**	**1800**	***2.1917***	**0.1361**	**0.2354**	93.43	1.37	1.46	54.8	245.0	**0.78**	**0.75**	**0.768**	121.64	1.78	3.56	**24.1**	1.762	0.027			
2296	JIF a011	1800	2.4885	0.2295	0.2110	72.85	1.09	1.50	36.9	173.6	0.78	0.75	0.773	94.25	1.41	2.82	38.5	0.936	0.015			
2816	**JIFa013**	**1800**	0.4872	0.0519	0.0702	58.31	0.95	1.62	37.9	122.1	0.67	0.63	0.658	88.63	1.44	2.88	37.0	1.378	0.029			
2818	JIFa014	1800	0.4102	0.0348	0.0836	61.64	1.49	2.42	51.5	214.9	0.65	0.60	0.630	97.91	2.36	4.73	36.1	2.448	0.085	67.3	9.1	18.2
									43.9	234.8												
2230	JIP a002	800	1.0277	0.1750	0.0798	43.45	0.78	1.81	47.4	208.4	0.76	0.73	0.761	57.13	1.03	2.06	27.7	0.465	0.015			
2229	JIP a003	800	1.7869	0.2788	0.1043	48.23	0.88	1.83	35.4	114.4	0.76	0.73	0.758	63.65	1.17	2.33	45.1	0.381	0.012			
2235	**JIP a006**	**800**	***2.0970***	**0.2461**	**0.0143**	68.71	1.30	1.89	73.5	182.4	**0.85**	**0.83**	**0.849**	80.96	1.53	3.06	**11.1**	0.059	0.003			
2236	JIP a007	800	0.2104	0.0492	0.0090	33.60	0.80	2.37			0.78	0.75	0.775	43.33	1.03	2.05	6.5	0.186	0.014			
2238	JIP a008	800	0.6129	0.1416	0.0289	33.87	0.69	2.05			0.78	0.75	0.777	43.60	0.89	1.79	20.5	0.208	0.007			
2528	JIP a009	800	0.1513	0.0448	0.0106	26.26	0.51	1.92	57.1	178.8	0.74	0.70	0.733	35.84	0.69	1.38	12.2	0.241	0.010			
2524	JIP a010	800	1.5451	0.2670	0.1075	43.30	0.66	1.53	63.0	261.1	0.77	0.74	0.768	56.36	0.86	1.72	37.4	0.410	0.007			
2906	JIP a011	800	1.9523	0.2978	0.1174	49.12	0.72	1.47	*59.7*	*269.8*	0.74	0.71	0.739	66.42	0.98	1.96	72.2	0.402	0.007			
2908	JIP a012	800	0.2631	0.0533	0.0257	36.36	0.72	1.98	62.8	221.9	0.75	0.72	0.748	48.61	0.96	1.93	12.2	0.492	0.013			
2912	**JIP a013**	800	1.5355	0.2479	0.1699	43.70	0.63	1.44	41.5	129.8	0.75	0.72	0.747	58.50	0.84	1.69	47.9	0.698	0.010			
2914	JIP a014	800	0.5721	0.1264	0.0621	33.27	0.56	1.67	38.2	124.7	0.73	0.70	0.728	45.68	0.76	1.53	36.1	0.500	0.012	94.6	4.7	9.3
2177	JID a003	600	0.6981	0.1510	0.0669	34.32	0.66	1.92			0.67	0.63	0.666	51.56	0.99	1.98	70.0	0.451	0.015			
2181	**JID a004**	600	3.4278	0.4329	0.2307	57.57	1.01	1.75	55.3	276.7	0.76	0.73	0.754	76.33	1.34	2.68	80.1	0.543	0.012			
2183	JID a005	600	1.5919	0.2588	0.1142	45.65	0.82	1.80	54.4	275.5	0.66	0.61	0.651	70.13	1.26	2.53	146.7	0.450	0.011			
2219	JID a006	600	0.9400	0.1265	0.1065	50.79	0.95	1.88	*99.2*	*277.6*	0.64	0.60	0.635	79.99	1.50	3.00	104.3	0.858	0.024			
2220	JID a007	600	2.9181	0.3712	0.2698	54.94	0.95	1.74	59.7	269.8	0.74	0.71	0.736	74.69	1.30	2.59	92.5	0.740	0.020			
2221	JID a008	600	2.1314	0.3286	0.3910	41.52	0.71	1.72	62.8	221.9	0.71	0.67	0.702	59.16	1.02	2.03	112.5	1.212	0.030			
2538	**JID a010**	**600**	2.2411	0.3330	0.2103	47.98	0.68	1.42	53.2	165.2	0.72	0.69	0.718	66.84	0.95	1.90	98.7	0.643	0.010			
2510	JID a011	600	0.3752	0.0679	0.0327	40.66	0.73	1.79	57.0	290.8	0.62	0.57	0.615	66.06	1.18	2.37	63.8	0.490	0.012			
2512	**JID a012**	**600**	2.6090	0.3916	0.2276	48.00	0.69	1.43			0.79	0.77	0.790	60.73	0.87	1.74	54.6	0.592	0.009			
2918	**JID a014**	**600**	0.7865	0.1069	0.0746	51.74	0.79	1.52			0.65	0.60	0.639	80.93	1.23	2.47	82.7	0.711	0.011			
2920	JID a015	600	0.3882	0.0757	0.0104	40.69	0.64	1.57	39.3	121.2	0.69	0.65	0.690	58.97	0.93	1.85	30.0	0.139	0.009	52.8	9.0	18.0
									75.7	297.7												
2169	JMG a001	200	0.1030	0.0231	0.0108	32.97	1.79	5.44	61.4	183.5	0.65	0.61	0.646	51.05	2.78	5.55	16.6	0.477	0.070			
2170	JMG a002	200	1.1016	0.1738	0.1276	44.28	1.00	2.25	66.7	271.6	0.82	0.79	0.814	54.42	1.23	2.45	14.5	0.748	0.029			
2173	JMG a003	200	0.2618	0.0551	0.0248	35.20	0.84	2.38	*81.7*	*442.7*	0.77	0.73	0.763	46.14	1.10	2.19	10.7	0.458	0.027			
2174	JMG a004	200	0.7688	0.1364	0.0904	39.96	0.74	1.85			0.80	0.77	0.792	50.47	0.94	1.87	15.8	0.675	0.015			
2175	**JMG a005**	**200**	***2.1505***	**0.3016**	**0.1359**	52.76	1.09	2.07			**0.84**	**0.82**	**0.836**	63.11	1.31	2.62	**13.7**	0.459	0.018	50.5	3.4	6.8
									62.0	150.7												
									38.8	147.1												
2168	JHG a001	1750	0.7151	0.0813	0.2257	43.60	0.75	1.72	63.3	230.3	0.72	0.68	0.699	62.38	1.07	2.14	41.7	2.829	0.067			
2197	**JHG a002**	**1750**	**1.5991**	**0.0913**	**0.2640**	85.16	1.52	1.78	59.6	160.7	**0.70**	**0.66**	**0.687**	123.99	2.21	4.42	**60.2**	2.946	0.078			
2198	JHG a003	1750	0.2350	0.0395	0.1131	29.13	0.56	1.94	43.7	195.7	0.66	0.61	0.636	45.77	0.89	1.77	44.1	2.914	0.086			
2199	**JHG a004**	**1750**	**0.6888**	**0.0505**	**0.1746**	61.59	1.08	1.76	58.5	147.5	**0.66**	**0.62**	**0.644**	95.70	1.69	3.37	**55.0**	3.525	0.088			
2200	JHG a005	1750	0.1707	0.0271	0.0674	32.56	0.67	2.05	53.6	143.7	0.62	0.57	0.600	54.31	1.11	2.23	38.9	2.529	0.080			
2380	**JHG a006**	**1750**	**0.3415**	**0.0208**	**0.0520**	84.54	1.91	2.26	*58.3*	*152.1*	**0.62**	**0.57**	**0.599**	141.12	3.20	6.39	**31.5**	2.551	0.088			
2526	JHG a007	1750	0.0262	0.0350	0.0065	5.90	0.15	2.59			0.64	0.59	0.636	9.28	0.24	0.48	26.2	0.188	0.010	39.3	7.3	14.5
2205	JHI a003	1700	0.4532	0.0557	0.1011	46.71	0.86	1.84	47.2	174.7	0.78	0.74	0.765	61.04	1.12	2.24	10.8	1.849	0.055			
2206	JHI a005	1700	0.7270	0.1730	0.0867	30.83	0.57	1.86	48.4	131.5	0.77	0.74	0.763	40.40	0.75	1.51	31.2	0.510	0.015			
2222	JHI a006	1700	3.0968	0.4064	0.7205	44.05	0.72	1.62	42.0	102.7	0.74	0.71	0.730	60.36	0.98	1.96	128.6	1.806	0.038			
2240	**JHI a006**	**1700**	***2.3232***	**0.1693**	**0.0521**	104.28	2.01	1.93	42.5	111.2	**0.83**	**0.80**	**0.825**	126.44	2.44	4.88	**12.4**	0.313	0.009			
2223	JHI a007	1700	1.0328	0.1957	0.0553	40.54	0.77	1.89	36.1	102.8	0.76	0.73	0.755	53.69	1.01	2.03	39.4	0.288	0.010	54.2	8.3	16.6
									37.9	88.2												
2207	JMZ a001	1150	0.2153	0.0408	0.0414	34.95	0.67	1.91	37.4	120.9	0.76	0.72	0.751	46.57	0.89	1.78	10.6	1.034	0.033			
2209	JMZ a002	1150	0.1699	0.0360	0.0340	31.62	0.79	2.50			0.66	0.62	0.652	48.52	1.21	2.43	24.0	0.962	0.035			
2212	JMZ a003	1150	0.5642	0.1299	0.1550	27.82	0.48	1.74			0.78	0.75	0.774	35.92	0.63	1.25	21.8	1.215	0.029			
2213	JMZ a004	1150	0.2597	0.0721	0.0502	25.39	0.57	2.25	59.8	248.5	0.76	0.72	0.749	33.88	0.76	1.52	17.8	0.709	0.056			
2226	**JMZ a006**	**1150**	**0.4696**	**0.0448**	**0.0384**	71.37	1.52	2.13	59.2	213.9	**0.70**	**0.66**	**0.696**	102.59	2.18	4.36	**17.4**	0.874	0.028			
2482	JMZ a006	1150	0.1837	0.0573	0.0429	22.37	0.34	1.52	52.1	199.2	0.75	0.71	0.741	30.20	0.46	0.92	16.2	0.763	0.014			
2486	JMZ a007	1150	0.2391	0.0563	0.0436	29.47	0.49	1.66	*85.2*	*244.0*	0.73	0.69	0.723	40.78	0.68	1.36	19.5	0.790	0.016			
2536	**JMZ a008**	**1150**	***0.9471***	**0.1022**	**0.0764**	64.47	1.07	1.66	57.5	194.3	**0.75**	**0.71**	**0.742**	86.91	1.44	2.88	**28.1**	0.762	0.016	53.9	9.6	19.1
2937	JJWa001	100	0.0026	0.0002	0.0003	78.79	51.01	64.74	nd		-	-	-	78.79	51.01	102.02		1.667	3.046			

APPENDIX III

ZIRCON (U-TH)/HE DATA

#	Sample	Elevation	[^{4}He]	[^{238}U]	[^{232}Th]	Raw Age	1σ	% 1σ	R1	R2	L	H1	H2	^{238}UF$_T$	^{232}ThF$_T$	Mean F$_T$	Age F$_{T\,corr}$	1σ	2σ	[eU]	Th/U	1σ	Av. Age	1 SD Ma	2 SD Ma
57		m	ncm^3	ng	ng	Ma	Ma		μm	μm	μm	μm	μm				Ma	Ma	Ma	ppm			Ma		
																						Apatite Zircon			
1848	**ESPR z001**	**3450**	24.2860	1.4477	0.4710	**126.70**	**2.07**	**1.63**	37.1	31.1	170.3	39.1	28.8	0.717	0.682	0.714	**177.54**	**2.90**	**5.80**	585	0.331	0.006			
1850	**ESPR z002**	**3450**	16.7848	0.9798	0.1513	**134.28**	**2.30**	**1.72**	44.1	41.3	150.6	34.8	28.7	0.756	0.725	0.754	**178.19**	**3.06**	**6.12**	279	0.157	0.004			
1998	**ESPR z003**	**3450**	25.7793	1.5533	2.8614	**94.50**	**1.37**	**1.45**	24.2	27.6	201.7	20.1	30.3	0.662	0.620	0.648	**145.74**	**2.12**	**4.23**	1072	1.876	0.031			
2000	ESPR z004	3450	20.3097	1.2615	0.4044	**121.78**	**1.97**	**1.62**	39.6	46.0	169.0	44.5	18.4	0.762	0.731	0.759	**160.51**	**2.59**	**5.19**	317	0.326	0.006	177.9	0.5	0.9
1796	**JIF z001**	**1800**	239.8668	1.1449	2.9507	**996.88**	**16.34**	**1.64**	48.2	46.7	357.5	39.3	46.0	0.808	0.783	0.798	**1249.32**	**20.48**	**40.96**	147	2.625	0.050			
1798	**JIF z004**	**1800**	286.2935	2.1384	1.3190	**887.22**	**14.48**	**1.63**	50.4	53.7	306.1	34.5	50.4	0.818	0.794	0.814	**1089.57**	**17.78**	**35.56**	196	0.628	0.010			
1800	**JIF z005**	**1800**	174.1415	2.1303	0.7115	**590.24**	**9.76**	**1.65**	43.7	49.9	351.5	45.5	41.2	0.805	0.779	0.802	**736.15**	**12.17**	**24.34**	194	0.340	0.006			
1802	**JIF z006**	**1800**	84.5042	4.5411	1.2454	**141.93**	**2.39**	**1.68**	46.5	45.7	288.1	41.9	35.5	0.798	0.772	0.796	**178.40**	**3.00**	**6.00**	520	0.279	0.005			
1806	**JIF z007**	**1800**	131.7569	6.5664	2.0529	**151.63**	**2.51**	**1.66**	53.1	49.0	323.3	61.3	45.8	0.815	0.791	0.813	**186.56**	**3.09**	**6.18**	583	0.318	0.005	182.5	5.8	11.5
1896	**JIP z001**	**800**	850.6884	18.0752	5.3239	**350.57**	**5.85**	**1.67**	73.0	72.8	508.1	68.0	59.7	0.872	0.855	0.870	**403.00**	**6.73**	**13.45**	466	0.300	0.005			
2137	**JIP z002**	**800**	273.5090	7.5945	1.5905	**275.22**	**4.22**	**1.53**	47.0	54.7	352.0	43.5	37.1	0.818	0.794	0.816	**337.28**	**5.17**	**10.33**	562	0.213	0.004			
2139	**JIP z003**	**800**	291.1032	8.6917	2.4696	**252.33**	**3.67**	**1.45**	56.5	50.5	322.1	41.3	43.7	0.824	0.800	0.821	**307.26**	**4.47**	**8.93**	662	0.289	0.004			
2141	JIP z004	800	213.4905	7.3251	2.5652	**217.16**	**3.22**	**1.48**	54.3	56.4	419.7	40.4	49.9	0.834	0.813	0.832	**261.00**	**3.87**	**7.74**	390	0.357	0.005			
2143	**JIP z005**	**800**	650.6700	19.9021	3.9197	**251.10**	**3.75**	**1.49**	60.7	60.0	435.2	63.4	56.8	0.846	0.826	0.845	**297.33**	**4.44**	**8.88**	872	0.201	0.003			
2435	**JIP z006**	**800**	157.7572	4.6535	1.0772	**258.22**	**4.02**	**1.56**	41.5	44.4	272.7	27.5	33.8	0.785	0.757	0.782	**330.04**	**5.14**	**10.27**	622	0.236	0.005			
2437	**JIP z007**	**800**	134.6440	3.3015	1.2359	**300.04**	**4.63**	**1.54**	52.2	49.8	236.8	43.3	44.9	0.806	0.781	0.803	**373.63**	**5.77**	**11.54**	421	0.381	0.007			
2439	**JIP z008**	**800**	236.6776	5.5218	0.8740	**329.59**	**5.38**	**1.63**	46.1	56.9	288.0	48.7	40.6	0.813	0.789	0.811	**406.23**	**6.63**	**13.26**	517	0.161	0.003	339.5	51.7	103.4
1884	**JID z001**	**600**	271.2759	81.3517	48.3855	**24.00**	**0.38**	**1.58**	45.9	51.1	334.4	57.2	45.2	0.809	0.784	0.805	**29.83**	**0.47**	**0.94**	8028	0.606	0.010			
1886	**JID z002**	**600**	221.0112	45.6197	7.8873	**38.15**	**0.62**	**1.63**	59.5	64.9	340.9	53.6	51.5	0.845	0.824	0.843	**45.24**	**0.74**	**1.48**	2455	0.176	0.003			
1878	**JID z003**	**600**	223.2090	48.3647	18.0353	**34.78**	**0.57**	**1.64**	56.5	51.7	350.8	61.4	63.4	0.825	0.802	0.823	**42.29**	**0.69**	**1.38**	3642	0.380	0.006			
1892	**JID z005**	**600**	481.0415	64.5297	15.3141	**57.76**	**0.97**	**1.68**	65.1	57.4	272.4	51.0	69.6	0.833	0.811	0.831	**69.47**	**1.16**	**2.33**	5138	0.242	0.004			
1894	JID z006	600	431.6344	88.1543	29.1455	**37.24**	**0.65**	**1.75**	58.0	53.2	262.3	42.3	50.4	0.822	0.799	0.820	**45.43**	**0.79**	**1.59**	8315	0.337	0.006			
2395	JID z007	600	130.1822	21.4784	1.8032	**48.67**	**0.79**	**1.61**	32.9	32.1	346.1	35.6	29.2	0.735	0.701	0.733	**66.42**	**1.07**	**2.14**	3711	0.086	0.002			
2397	JID z008	600	228.7636	62.0682	18.7243	**28.23**	**0.45**	**1.60**	38.9	40.2	265.1	27.0	21.8	0.770	0.740	0.767	**36.82**	**0.59**	**1.18**	9875	0.307	0.005			
2481	JID z009	600	145.3941	16.6633	2.4535	**68.92**	**1.15**	**1.67**	45.0	43.8	247.3	36.3	46.0	0.786	0.758	0.784	**87.90**	**1.47**	**2.93**	2461	0.150	0.003	52.9	19.6	39.3
1862	**JMG z001**	**200**	65.7933	7.0049	1.3857	**73.32**	**1.23**	**1.68**	47.4	40.1	244.2	41.0	35.1	0.782	0.754	0.780	**94.00**	**1.57**	**3.15**	1082	0.201	0.003			
1864	**JMG z002**	**200**	153.1691	13.8133	2.2139	**87.18**	**1.47**	**1.68**	56.4	48.1	317.1	63.5	51.5	0.817	0.793	0.815	**106.96**	**1.80**	**3.60**	1191	0.163	0.003			
1866	**JMG z003**	**200**	261.8264	6.7496	1.4094	**295.91**	**4.91**	**1.66**	61.1	63.4	355.1	99.1	73.9	0.841	0.820	0.839	**352.70**	**5.85**	**11.70**	413	0.213	0.004			
1868	**JMG z004**	**200**	253.0315	16.3001	4.3181	**118.89**	**1.99**	**1.68**	52.4	51.8	468.7	78.9	62.0	0.826	0.803	0.824	**144.37**	**2.42**	**4.84**	922	0.270	0.005			
1870	**JMG z005**	**200**	131.2358	7.1752	2.3395	**137.98**	**2.32**	**1.68**	47.8	45.0	374.8	46.4	57.1	0.804	0.779	0.802	**172.13**	**2.89**	**5.79**	635	0.332	0.006			
2441	**JMG z006**	**200**	159.1660	3.7157	0.7678	**325.99**	**5.27**	**1.62**	53.3	52.4	317.2	55.4	59.8	0.820	0.796	0.818	**398.65**	**6.45**	**12.90**	314	0.210	0.004			
2443	**JMG z007**	**200**	204.4421	5.4426	0.7910	**290.75**	**4.77**	**1.64**	55.8	53.3	323.1	67.1	48.2	0.825	0.802	0.823	**353.23**	**5.80**	**11.59**	416	0.148	0.003	100.5	9.2	18.3
1814	**JHG z002**	**1750**	49.6139	47.2096	3.4134	**8.49**	**0.14**	**1.62**	35.2	32.7	191.0	37.6	32.1	0.724	0.689	0.722	**11.76**	**0.19**	**0.38**	15629	0.074	0.001			
1816	**JHG z003**	**1750**	42.2735	21.8430	1.7289	**15.60**	**0.25**	**1.62**	32.5	34.2	164.4	28.0	26.5	0.716	0.680	0.714	**21.86**	**0.35**	**0.71**	8462	0.081	0.002			
1820	**JHG z004**	**1750**	60.0333	172.2068	8.1148	**2.84**	**0.05**	**1.71**	41.4	37.2	197.5	35.3	26.0	0.757	0.725	0.755	**3.75**	**0.06**	**0.13**	39073	0.048	0.001			
1822	JHG z005/006	1750	24.0235	2.1629	1.3803	**78.87**	**1.30**	**1.65**	30.9	29.6	181.2	21.4	25.4	0.699	0.662	0.693	**113.79**	**1.88**	**3.75**	981	0.650	0.011			
1824	JHG z007	1750	45.7745	4.9262	2.1498	**68.88**	**1.12**	**1.63**	36.4	40.8	177.6	37.1	30.6	0.747	0.714	0.743	**92.75**	**1.51**	**3.01**	1493	0.444	0.007			
2368	JHG z008	1750	25.1138	1.0619	0.4993	**172.48**	**2.95**	**1.71**	30.7	26.1	134.0	24.5	20.1	0.667	0.625	0.661	**260.90**	**4.47**	**8.93**	765	0.479	0.008			
2393	JHGz009	1750	22.8953	2.4048	1.4587	**68.11**	**1.06**	**1.56**	28.1	29.8	170.0	25.6	25.6	0.685	0.646	0.679	**100.36**	**1.57**	**3.13**	1308	0.618	0.011	102.3	10.6	21.3
1780	**JHI z001**	**1700**	71.6948	8.5629	2.6809	**63.77**	**1.06**	**1.66**	47.5	49.3	246.7	78.9	80.6	0.785	0.757	0.782	**81.55**	**1.36**	**2.71**	1514	0.319	0.005			
1782	**JHI z002**	**1700**	98.5745	13.9651	4.9110	**53.36**	**0.87**	**1.63**	65.8	59.3	228.8	74.0	68.5	0.823	0.799	0.820	**65.08**	**1.06**	**2.13**	1567	0.358	0.006			
1788	**JHI z003**	**1700**	149.1233	5.5998	1.5586	**201.82**	**3.45**	**1.71**	44.2	56.4	228.4	63.2	55.0	0.795	0.768	0.792	**254.76**	**4.35**	**8.70**	865	0.283	0.005			
1794	JHI z005	1700	65.2569	12.7389	4.0605	**39.05**	**0.64**	**1.63**	52.4	63.3	234.1	60.0	48.9	0.819	0.796	0.817	**47.80**	**0.78**	**1.56**	1385	0.325	0.005			
2648	JHI z006	1700	379.9546	1.7287	1.1581	**1372.26**	**24.17**	**1.76**	67.4	74.8	266.3	64.6	49.6	0.851	0.832	0.848	**1618.49**	**28.51**	**57.01**	113	0.682	0.010			
2652	JHI z007	1700	68.3320	0.5128	0.2677	**898.61**	**15.45**	**1.72**	33.5	45.7	186.1	32.5	35.4	0.750	0.718	0.745	**1205.83**	**20.73**	**41.46**	145	0.532	0.009	64.8	16.9	33.8
1770	**JMZ z002**	**1150**	696.8488	3.1047	1.7618	**1420.74**	**25.51**	**1.80**	102.1	92.1	588.1	79.2	132.7	0.899	0.886	0.897	**1583.11**	**28.43**	**56.85**	45	0.578	0.010			
1772	**JMZ z003**	**1150**	157.5249	2.0118	1.1114	**542.94**	**9.38**	**1.73**	71.9	66.8	404.3	81.7	96.1	0.858	0.840	0.856	**634.60**	**10.96**	**21.92**	90	0.563	0.010			
1774	**JMZ z004**	**1150**	260.9304	2.5338	1.6570	**690.31**	**11.84**	**1.72**	84.3	65.7	497.8	69.2	86.5	0.872	0.855	0.869	**794.41**	**13.63**	**27.25**	73	0.666	0.011			
2586	**JMZ z006**	**1150**	76.4279	8.3325	0.8681	**73.14**	**1.22**	**1.66**	39.9	38.6	297.0	63.9	67.8	0.763	0.733	0.761	**96.09**	**1.60**	**3.20**	1433	0.106	0.002			
2584	JMZ z007	1150	19.4914	3.4010	0.2957	**45.99**	**0.78**	**1.69**	35.0	29.5	258.9	38.5	38.2	0.722	0.687	0.720	**63.85**	**1.08**	**2.16**	877	0.089	0.002			
2656	**JMZ z009**	**1150**	44.3022	0.5573	0.0580	**602.39**	**9.77**	**1.62**	42.3	44.7	335.9	56.0	51.8	0.790	0.763	0.788	**764.22**	**12.39**	**24.79**	62	0.106	0.004			
2658	**JMZ z010**	**1150**	29.1505	0.5772	0.0685	**389.56**	**6.42**	**1.65**	36.9	32.4	246.4	33.6	47.9	0.737	0.703	0.735	**530.24**	**8.73**	**17.47**	140	0.121	0.004	80.0	22.8	45.6
2145	JJW z001	100	9.5660	2.2096	0.6271	**33.28**	**0.50**	**1.50**	26.3	32.1	187.5	31.1	42.0	0.684	0.645	0.680	**48.90**	**0.73**	**1.46**	1089	0.289	0.005			
2217	**JJW z003**	**100**	2.1371	0.4802	0.2715	**32.21**	**0.52**	**1.61**	30.2	26.0	152.9	32.4	24.1	0.669	0.628	0.663	**48.58**	**0.78**	**1.57**	325	0.576	0.011			
1826	JJW z004	100	5.0378	0.9613	0.4192	**38.95**	**0.62**	**1.59**	34.5	39.9	154.5	26.8	28.8	0.734	0.700	0.729	**53.41**	**0.85**	**1.70**	354	0.444	0.008			
1828	JJW z005	100	1.2128	0.3312	0.0727	**28.56**	**0.52**	**1.81**	28.0	24.4	110.0	20.0	23.6	0.632	0.587	0.628	**45.44**	**0.82**	**1.64**	341	0.224	0.007			
2221	JJW z006	100	2.3314	0.7142	0.2273	**24.92**	**0.37**	**1.50**	33.2	29.0	130.9	22.2	22.1	0.687	0.648	0.683	**36.48**	**0.55**	**1.10**	427	0.324	0.007	49.1	3.3	6.6